PARKINSON'S DISEASE

Transcranial ultrasound stimulation of motor networks in Parkinson's disease informed by local field potential dynamics

Can Sarica[1,2]†, Ghazaleh Darmani[1,2]†, Hamidreza Ramezanpour[3]†, Marcus Callister[4], Brendan Santyr[1,2], Talyta Grippe[4], Regina Annirood[2], Nasem Raies[2], Jean-Francois Nankoo[2], Nardin Samuel[4], Mandy Yi Rong Ding[2], Artur Vetkas[5], Anton Fomenko[1], Jeffrey D. Schall[3], Mojgan Hodaie[1,2,6], Suneil K. Kalia[1,2,6,7], Agessandro Abrahao[8,9,10], Renato P. Munhoz[2,4], Alfonso Fasano[2,4,6,7], Samuel Pichardo[11], Robert Chen[2,4,6]‡, Andres M. Lozano[1,2,6]*‡

Transcranial ultrasound stimulation (TUS) is a promising noninvasive technique for modulating deep brain targets and circuits with high spatial precision. For its successful clinical translation, confirmation of target engagement, together with a deeper understanding of the effects of TUS, is essential. To advance these goals, we obtained direct measures of neural activity using electrodes implanted in the subthalamic nucleus (STN) in patients with Parkinson's disease (PD) during TUS of deep and superficial targets, guided by magnetic resonance imaging–based acoustic modeling and real-time neuronavigation. Seventeen patients were studied in the on-medication and off–deep brain stimulation states. Each patient received one active and one sham session in a randomized order, and 13 of 17 patients (76%) completed a third session, which was always active. Each active condition targeted a single site—either the primary motor cortex (M1), the globus pallidus internus (GPi), or the occipital cortex (control site)—with 10 patients per active target. TUS effects on the STN were found to be target specific. Stimulation of the M1 reduced STN beta oscillation activity compared with sham stimulation and was associated with improvements in motor signs. These effects were brain state specific, showing distinct modulation patterns at rest versus during movement. In contrast, TUS targeting the GPi increased beta activity relative to control conditions and did not improve motor signs. Our results provide mechanistic evidence that TUS can safely and selectively modulate pathological brain rhythms in the STN in PD, supporting its potential as a targeted, noninvasive therapeutic modality.

INTRODUCTION

Neuromodulation can target pathological brain circuit activity through both invasive and noninvasive techniques (*1*). Deep brain stimulation (DBS) is an established invasive technique that can produce meaningful therapeutic benefits but that carries risks of surgical complications and requires substantial clinical and financial resources (*2*). To date, no noninvasive technique has demonstrated clinical effects on deep structures as robust as those achieved by DBS (*1*). Transcranial ultrasound stimulation (TUS) is an innovative and relatively affordable noninvasive technique capable of modulating deep brain circuits, with the potential to either complement or serve as an alternative to DBS (*3*).

However, the clinical translation of TUS remains challenging due to its poorly understood effects on neural elements, limited knowledge of dose-response relationships, and variability in outcomes related to differences in skull penetrance across individuals. Proposed mechanisms to explain the effects of ultrasound include direct activation of mechanosensitive ion channels, capacitive changes in the cell membrane, indirect neuromodulation through astrocytes, and thermal effects (*4*–*16*). The nonuniform spatial distribution of ion channels and cellular variability within the brain constitute the first major challenges to clinical translation. The second major challenge is the dose-dependent nature of ultrasound, where variations in parameters—such as intensity, frequency, and pulse duration—can alter both the nature (inhibitory or excitatory) and duration of effects, as demonstrated in preclinical models (*17*–*23*) and humans (*24*–*27*). Modulatory effects also depend on the individual's behavioral state, such as being anesthetized, resting, or active (*21*, *28*–*32*). The skull introduces additional complexity by causing aberration, attenuation, and distortion of the ultrasound beam—effects that vary not only between species but also across different regions within the same skull. Successful TUS requires selecting the correct network to modulate, identifying the most ultrasound responsive hub(s) within the network, optimizing the dose and behavioral state for the desired effect, and precise target engagement by individually calculating skull penetrance to compensate for skull-induced distortions.

The high degrees of freedom required for successful TUS demand rigorous human testing for clinical translation. Although noninvasive methods like electroencephalography and functional magnetic resonance imaging (MRI) offer useful insights, invasive

[1]Division of Neurosurgery, Department of Surgery, University of Toronto, Toronto, ON M5T 2S8, Canada. [2]Krembil Research Institute, University Health Network, Toronto, ON M5T 0S8, Canada. [3]Department of Biology, York University, Toronto, ON M3J 1L3, Canada. [4]Edmond J. Safra Program in Parkinson's Disease Morton and Gloria Shulman Movement Disorders Clinic, Toronto Western Hospital, and Division of Neurology, University of Toronto, Toronto, ON M5T 2S8, Canada. [5]Department of Clinical Neuroscience, Section for Neurosurgery, Karolinska Institutet, 171 76 Stockholm, Sweden. [6]Center for Advancing Neurotechnological Innovation to Application (CRANIA), Toronto, ON M5T 2S8, Canada. [7]KITE, University Health Network, Toronto, ON M5T 2S8, Canada. [8]Division of Neurology, Department of Medicine, Sunnybrook Health Sciences Centre, University of Toronto, Toronto, ON M4N 3M5, Canada. [9]Harquail Centre for Neuromodulation, Sunnybrook Research Institute, Toronto, ON M4N 3M5, Canada. [10]Hurvitz Brain Sciences Program, Sunnybrook Research Institute, Toronto, ON M4N 3M5, Canada. [11]Department of Radiology, Cumming School of Medicine, University of Calgary, Calgary, AB T2N 2T8, Canada.
†These authors contributed equally to this work.
‡These authors contributed equally to this work.
*Corresponding author. Email: lozano@uhnresearch.ca

high-fidelity spatiotemporal measurements, such as local field potential (LFP) recordings, allow direct analysis of TUS effects on neural oscillations. This is particularly relevant because specific frequency bands serve as disease-related biomarkers; for example, exaggerated beta-band activity in the basal ganglia is a hallmark of Parkinson's disease (PD) (*33*). Given this, attenuating pathological beta activity may offer meaningful therapeutic benefits. For instance, in the context of PD pathophysiology, increasing facilitatory drive at primary motor cortex (M1) and reducing excessive output from an overactive globus pallidus internus (GPi) would both be expected to suppress pathological subthalamic nucleus (STN) beta through distinct cortical–basal ganglia pathways—highlighting beta suppression as a robust downstream biomarker of circuit modulation (*33*). However, integrating TUS with LFP recordings introduces unique challenges. Using externalized electrodes shortly after DBS surgery carries a risk of cavitation and tissue damage because of residual intracranial air. In contrast, modern DBS systems enable chronic LFP recordings, allowing safer TUS investigations to be conducted weeks after surgery (*34*). We addressed the safety concerns of this TUS-LFP approach in patients with DBS implants through a two-step process: first with an ex vivo safety study (*35*) and subsequently in a pilot human trial in which TUS was applied directly to target the location of DBS contacts (*36*). Upon confirming safety in humans, we proceeded to investigate whether this method could guide the clinical translation of TUS in patients with PD.

We hypothesized that STN LFP changes in response to TUS could reveal key characteristics of its effects, including magnitude, directionality, and duration of postsonication—insights that could help guide desired clinical outcomes. To test this, LFP responses were recorded under four TUS conditions targeting motor and nonmotor circuits. Each patient underwent one active and one sham session in a randomized, single blinded order, and a subset (13 of 17) completed a third session, which was always active. The active conditions targeted the GPi, M1, or occipital cortex (Occ; active control), whereas the fourth condition was an inactive sham. All stimulations were guided by personalized acoustic simulations to account for skull-induced distortions. STN LFP recordings were acquired during sonication and at 10-, 30-, and 45-min intervals postsonication, both at rest and during a finger-tapping task to assess brain state–dependent effects.

RESULTS

Neural recordings of STN activity during TUS

STN LFP changes and their clinical correlates in response to four different TUS conditions were investigated in 17 patients with PD (Table 1), all implanted with bilateral DBS systems equipped with a recording-capable Percept PC implantable pulse generator (IPG) (Fig. 1A). These changes were analyzed both during TUS at rest (online effects: T0) and after sonication at 10, 30, and 45 min during rest and movement (offline effects: T10, T30, and T45) (see study design in Fig. 1B). Each participant underwent one sham TUS session and one active TUS session, targeting the GPi, M1, or Occ, in randomized order. Some participants consented to a third session and were randomized to an additional active TUS session. Each active condition was designed to include 10 participants, whereas the sham TUS condition included all 17 participants. The theta-burst TUS (tbTUS) protocol—previously shown to modulate cortical excitability—was used across all conditions to enable target-specific comparisons (*24*, *36*, *37*).

Personalized transcranial acoustic simulations

Free-field acoustic simulations using BabelBrain software at a spatial peak pulse average intensity (I_{SPPA}) of 30 W/cm^2 were performed under water conditions for two focal depths—61 mm (representing the GPi) and 34 mm (representing cortical targets)—because 30 W/cm^2 is the maximum output available to end users on the NeuroFUS device. The results showed that the focal region along the beam trajectory was both shorter and narrower for superficial targets compared with a deeper one. Specifically, the full width at half maximum (FWHM) of the axial cross section measured 14.3 mm for M1/Occ and 26.4 mm for GPi, whereas the lateral FWHM measured 2.9 mm for M1/Occ and 3.7 mm for GPi (Fig. 2A). We obtained MRI images of the patients to perform personalized transcranial acoustic simulations using BabelBrain software. We simulated the in situ spatial intensity distributions and temperature elevations for each patient before each sonication session, accounting for skull-induced distortions. The optimized trajectories and corresponding pressure maps were coregistered onto each patient's native MRI using neuronavigation software to guide the procedure, as illustrated in Fig. 2B. The estimates of I_{SPPA} and mechanical index (MI) within the target areas varied substantially across sonication targets, with a linear mixed-effects model revealing a significant main effect of target for both I_{SPPA} [$\chi^2(2) = 26.29$, $P < 0.001$] and MI [$\chi^2(2) = 24.47$, $P < 0.001$] (Fig. 2C). The Occ had the highest values for both I_{SPPA} (5 ± 1.6 W/cm^2) and MI (0.48 ± 0.08), which were significantly higher than those observed in the M1 (3.2 ± 1.4 W/cm^2 and 0.38 ± 0.08, respectively; $P_{adj} < 0.001$ for both) and higher than those in the GPi for I_{SPPA} only (4.4 ± 1.2 W/cm^2 and 0.45 ± 0.07, respectively; $P_{adj} < 0.05$ for I_{SPPA} and $P_{adj} = 0.13$ for MI). The GPi values were also significantly higher than those in the M1 ($P_{adj} < 0.01$ for I_{SPPA} and $P_{adj} < 0.001$ for MI). The unadjusted mean distance to the GPi target was 55.6 ± 4.1 mm, whereas the adjusted mean distance, accounting for skull energy losses and beam distortions, was 56.9 ± 4.4 mm (Fig. 2D, left). The extent of transducer repositioning within the individual space, as determined by initial simulations, is illustrated in Fig. 2D (right). The maximum temperature rise varied significantly during GPi, M1, or Occ targeting across the skin [$\chi^2(2) = 16.44$, $P < 0.001$], skull [$\chi^2(2) = 19.59$, $P < 0.001$], and brain [$\chi^2(2) = 18.01$, $P < 0.001$]. However, the temperature increase remained below 0.19°C in the brain, 0.24°C in the skin, and 0.26°C in the skull, as detailed in Fig. 2E. Occ-tbTUS caused significantly less heating than GPi-tbTUS across all compartments ($P_{adj} < 0.001$) and less than M1-tbTUS in the skin and skull ($P_{adj} < 0.01$) but not in the brain ($P_{adj} = 0.18$). M1-tbTUS yielded lower heating than GPi-tbTUS only in the brain ($P_{adj} < 0.05$). The maximum temperature rise during the entire duration of the sonications, along with I_{SPPA} and MI predictions from simulations, remained well within conservative exposure ranges based on US Food and Drug Administration (FDA) diagnostic ultrasound guidelines and the consensus framework proposed by the International Transcranial Ultrasonic Stimulation Safety Standards (ITRUSST) Consortium (maximum temperature rise $\leq$ 2°C; MI ≤ 1.9; $I_{SPPA} \leq 190$ W/cm^2) (*38*).

Subjective changes and adverse events associated with TUS

We evaluated TUS-induced sensations and potential adverse events after each visit by asking patients, "did you experience anything unusual during TUS?" and "could you distinguish whether it was real or sham stimulation?," ensuring that blinding to the study condition was maintained. Across 47 sessions, patients reported subjective PD

Table 1. Patient characteristics. The levodopa equivalent daily dose (LEDD) was calculated as 100 mg of standard levodopa (L-dopa) = 133 mg of controlled-release levodopa = 303 mg of entacapone (ENT) = 100 mg of amantadine (AMA) = 1 mg of pramipexole (PRA) = 100 mg of rasagiline (RAS) = 5 mg of ropinirole = 3.3 mg of rotigotine (ROT) = 10 mg of selegiline = 100 mg of safinamide (SAF). AR, akinetic-rigid; DD, disease duration (years); E, equivalent; F, female; H&Y, Hoehn and Yahr; L, left; LID, levodopa-induced dyskinesias; M, male; R, right; S, symmetric; SSD, surgery-to-study duration (months); TD, tremor-dominant; U on, MDS-UPDRS (Movement Disorders Society Unified Parkinson's Disease Rating Scale) Part III Motor Examination Medication ON; the last row shows means ± SD values.

ID	Age	Sex	DD	SSD	Onset side–type	Late-stage most affected side–type	U on	H&Y	LID	LEDD (mg)	Medication	DBS leads	DBS parameters [active contacts/ amplitude (mA)/ pulse width (μs)/ frequency (Hz)]
01	72	F	10	2	L–TD	L–E	57	2	No	1682	ENT, L-dopa	SenSight	L: C+ 2–/2/60/130 R: C+ 10–/2/60/130
02	62	M	7	3	L–TD	R–AR	31	2	No	850	AMA, L-dopa	SenSight	L: C+ 3–/3/60/130 R: C+ 11–/2.5/60/130
03	74	M	24	79	R–AR	S–AR	68	2	No	975	AMA, L-dopa, PRA	3387	L: 3+ 2–/4.5/60/60 R: C+ 10–/3.8/60/60
04	66	M	7	52	R–AR	S–AR	56	3	Yes	550	AMA, L-dopa	3387	L: C+ 0–/4/60/110 R: C+ 10–/4.9/60/110
05	67	M	14	41	R–AR	L–AR	40	2	Yes	1750	AMA, L-dopa, PRA	3387	L: C+ 3–/6.5//C+ 2–/4.7/60/70 R: C+ 11–/6.1/60/70
06	62	M	11	13	L–TD	L–AR	43	2	No	500	L-dopa	SenSight	L: C+ 1–/2.8/60/180 R: C+ 10–/3.9/60/180
07	62	F	11	2	R–AR	R–AR	21	2	Yes	1270	L-dopa, ROT, SAF	SenSight	L: C+ 2–/1.5/60/130 R: C+ 10–/1.5/60/130
08	60	M	13	3	L–AR	R–E	17	2	No	900	L-dopa, PRA	SenSight	L: C+ 3–/3.2/50/130 R: C+ 10–/3.2/50/130
09	65	M	21	95	L–TD	L–E	50	2	No	1926	L-dopa	3387	L: C+ 2–/1.3/60/180 R: C+ 10–/4.7/60/180
10	68	M	12	42	R–TD	R–AR	54	3	No	1350	L-dopa	3387	L: C+ 0–/3.8//C+ 3–/4/60/100 R: C+ 11–/2.9/60/100
11	70	M	10	59	R–TD	L–AR	77	5	No	600	L-dopa	3387	L: C+ 3–/8.3/40/180 R: C+ 11–/3.2/60/180
12	70	M	16	3	L–TD	L–AR	42	2	No	1950	AMA, L-dopa, PRA	SenSight	L: C+ 1–/2/60/130 R: C+ 9–/2/60/130
13	61	M	11	2	L–TD	L–E	28	2	No	2225	AMA, L-dopa, PRA	SenSight	L: C+ 1–/1/60/130 R: C+ 10–/1/60/130
14	60	M	7	2	R–TD	R–AR	30	2	No	400	L-dopa	SenSight	L: C+ 2–/2.5/60/150 R: C+ 10–/1.5/60/150
15	76	M	18	70	R–AR	S–AR	32	2	Yes	1836	L-dopa, RAS, ROT	3387	L: C+ 2–3–/1.7/60/130 R: C+ 10–/3.5/40/130
16	66	M	6	2	R–TD	S–AR	17	2	Yes	1464	ENT, L-dopa	SenSight	L: C+ 2–/1/60/130 R: C+ 11–/1/60/130
17	40	M	8	2	L–TD	L - TD	50	2	No	575	L-dopa, PRA	SenSight	L: C+ 1–/3.3/40/160 R: C+ 10–/3.2/40/160
–	64.7 ± 8	–	12.1 ± 5.1	27.7 ± 32.5	–	–	41.9 ± 17.4	2*	–	1224 ± 599	–	–	–

*Median.

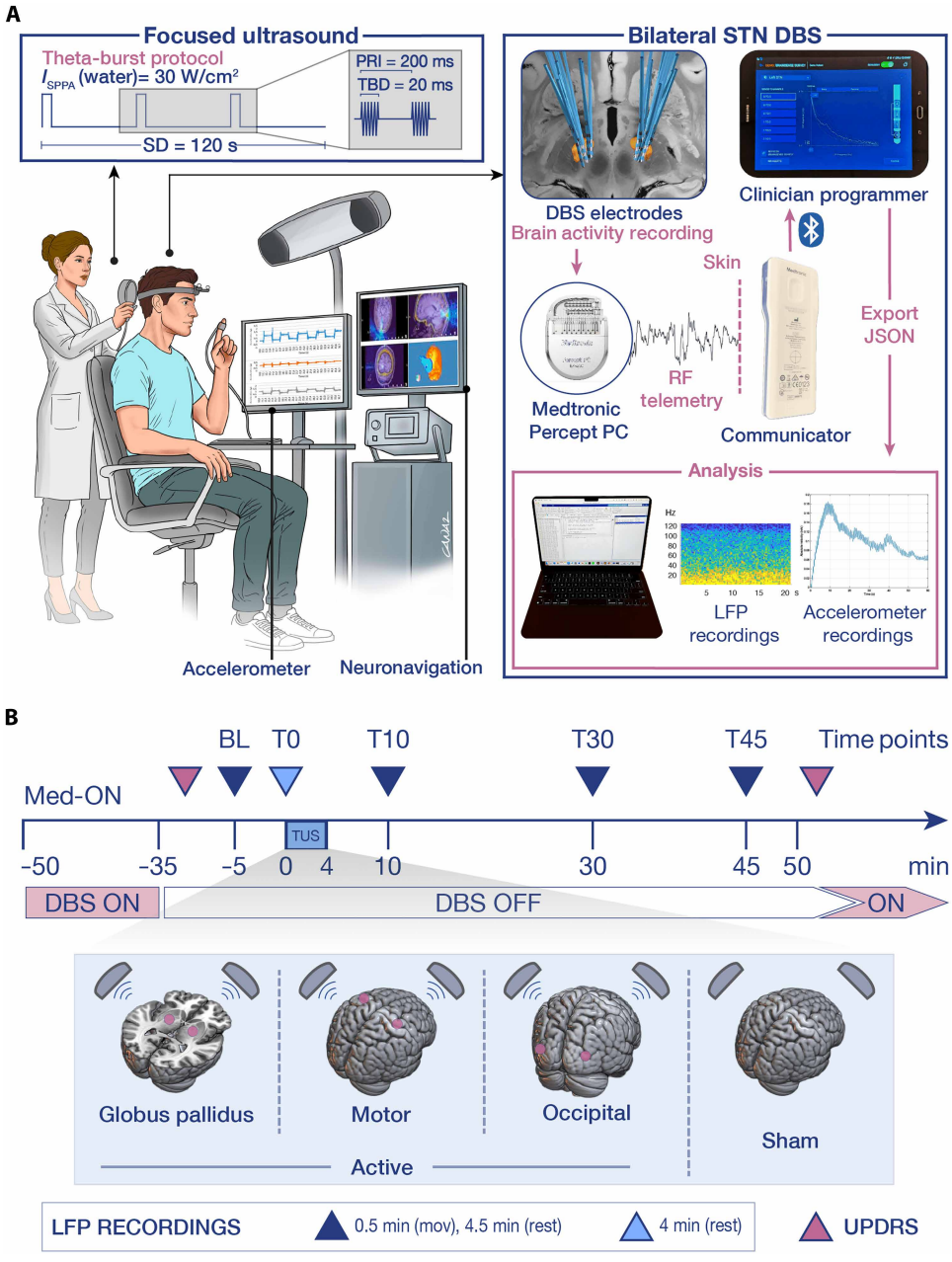

Fig. 1. Study design and timeline. (**A**) A schematic illustrates the TUS system and LFP recordings from the STN using a DBS device. A neuronavigation system was used to deliver TUS to specified targets of patients with Parkinson's disease using a theta burst protocol, lasting 120 s per hemisphere. Finger-tapping tasks were monitored using an accelerometer. (**B**) The timeline of a study visit included the MDS-UPDRS-III assessments performed at the beginning and end of each visit by a blinded neurologist, with video recordings reviewed for scoring by another blinded neurologist. Finger-tapping task was not performed during TUS delivery. Patients were already in their chronic Med-ON state when they took their scheduled levodopa dose 50 min before ultrasound. Sonication targets included the M1, GPi, and occipital cortex, along with a sham stimulation condition. BL, baseline; JSON, Javascript Object Notation file; Med, medication; min, minutes; PRI, pulse repetition interval; RF, radio frequency; SD, sonication duration; TBD, tone-burst duration.

symptom relief in five sessions (11%; two GPi, one M1, one occipital, and one sham) and sensations such as tingling, pain, or heating on the scalp in four sessions (9%; one GPi, one M1, and two occipital). One patient reported a tingling sensation in the right hand lasting a few seconds during left M1 sonication. No phosphenes were reported during any occipital stimulation sessions. Seven of 17 (41%) sham stimulation visits were guessed correctly, compared with 13 of 30 (43%) active stimulation visits. Binomial tests showed that guessing accuracy did not differ from chance for either sham ($P = 0.63$) or active ($P = 0.53$) sessions, and there was no systematic bias toward guessing "active" or "sham" ($P = 1.00$). A neurological examination assessing motor and sensory domains, cranial nerves, and mental state was conducted by a neurologist following the Movement Disorders Society Unified Parkinson's Disease Rating Scale, Part III (MDS-UPDRS-III) evaluations performed before and after each sonication session. No significant changes were observed between pre- and postsonication examinations. The day after each session, patients were contacted by telephone and asked, "did you experience any unpleasant condition related to the TUS session?" No adverse experiences were reported, except for fatigue in nine (19%) sessions.

tbTUS of the GPi, M1, and Occ differentially modulates STN LFPs

We modeled the DBS electrode placement for all patients in MNI space to visualize the contact locations relative to the STN (Fig. 3A). We found no statistically significant differences in baseline spectral power across the four conditions in theta, alpha, and beta bands at rest (Kruskal-Wallis test, 3 to 7 Hz: $P = 0.94$; 8 to 12 Hz: $P = 0.92$; 13 to 30 Hz: $P = 0.19$) (Fig. 3B). All conditions exhibited power dominance in the theta and alpha bands, with a pronounced peak in the 8- to 10-Hz range. We then analyzed changes in STN LFP power from baseline across the four sonication conditions during rest, pooling data from both hemispheres ($n = 20$ for GPi, M1, and Occ; $n = 34$ for sham) and four time points: T0, T10, T30, and T45 (Fig. 3C). Overall power in the 3- to 30-Hz range increased significantly across all conditions [Wilcoxon signed-rank test, false discovery rate (FDR)–adjusted $P < 0.001$ for all]. During M1 sonication, significant increases were observed in overall power for the

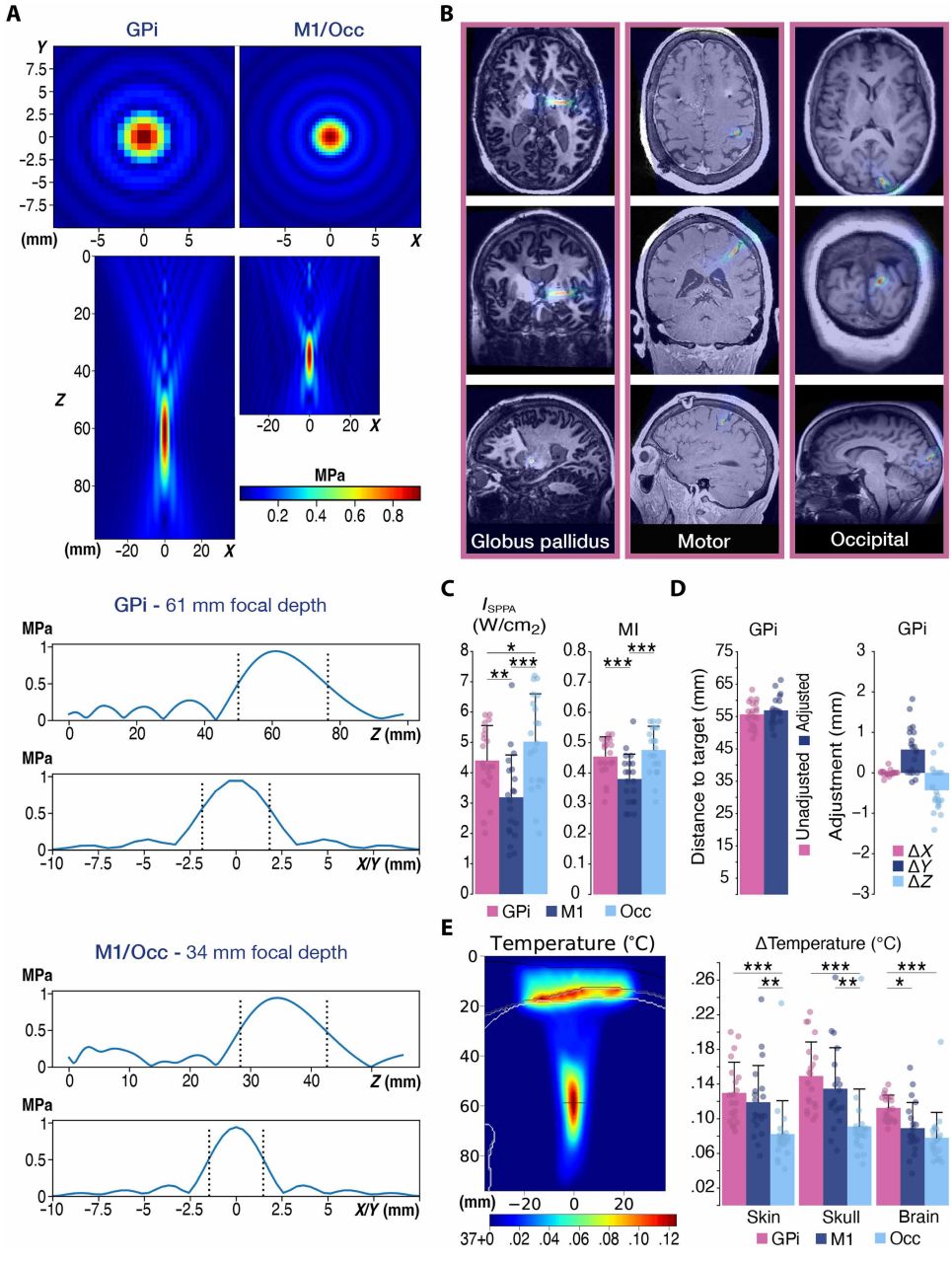

Fig. 2. Free-field and personalized transcranial acoustic simulations. (**A**) Free-field acoustic simulations displaying lateral (*x*/*y* axes; top) and axial (*z* axis; bottom) cross sections of acoustic pressure for target depths of 61 mm (GPi) and 34 mm (cortical targets). In the pressure profile plots (below), dotted lines mark the FWHM boundaries. (**B**) Pressure maps from individual simulations were overlaid on axial, coronal, and sagittal MRIs of S01 (left GPi and M1) and S07 (left Occ) as examples. (**C**) I_{SPPA} and MI values were reported across all three conditions. (**D**) The simulated sonication depth was compared with the unadjusted transducer-to-target distance. Transducer positions were adjusted along the *x*, *y*, and *z* axes to correct beam deviations. (**E**) An example temperature profile from S01's GPi-tbTUS session is shown (left), with the transducer outside the skull and ultrasound waves directed toward the target. Estimated mean temperature increases for the skin, skull, and brain tissue (right). Each bar in (C) to (E) is overlaid with 20 data points, corresponding to the 20 hemispheres of 10 patients. A linear mixed-effects model with FDR correction was used for intensity and temperature analyses. Data are presented as mean values, and error bars represent 1 SD. Statistical significance is denoted as follows: $*P < 0.05$; $**P < 0.01$; $***P < 0.001$.

theta and alpha bands (both $P_{adj} < 0.001$), whereas beta power changes were not significant ($P = 0.07$, $P_{adj} = 0.07$). In contrast, for the GPi, Occ, and sham conditions, overall power in the beta band increased significantly (GPi: $P_{adj} < 0.001$; Occ: $P_{adj} < 0.01$; sham: $P_{adj} < 0.001$), with no significant changes observed in the theta or alpha bands (Fig. 3C; see data file S1 for all *r* and *P* values).

tbTUS of M1 suppresses beta activity at rest after sham correction, whereas GPi enhances it

After computing STN LFP power changes for each condition (postsonication, pooled across time points and hemispheres, relative to baseline), we performed a paired subtraction of each patient's power change in the sham condition from their corresponding power change in the active sonication condition to isolate the specific effects of each sonication condition and account for sham effects and time-related changes. We found that the difference in power change during rest was 10.6 ± 1.7% 95% confidence interval [7.3 to 14.0%] ($r = 0.46$, $P_{adj} < 0.001$) between GPi and sham (GPi-sham), −8.7 ± 1.9% [−12.5 to −4.9%] ($r = -0.31$, $P_{adj} < 0.01$) between M1 and sham (M1-sham), and −5.5 ± 2.4% [−10.3 to −0.7%] ($r = -0.12$, $P_{adj} = 0.27$) between the occipital and sham (Occ-sham) (Fig. 4A, top row). Percent power change from baseline as a function of frequency is shown separately for all four postbaseline time points in Fig. 4A (middle row). We further examined power dynamics in the theta, alpha, and beta frequency bands. When all four postbaseline time points (T0, T10, T30, an T45) were combined, GPi-tbTUS significantly increased beta power (17.8 ± 4.4% [9.2 to 26.3%], $r = 0.35$, $P_{adj} < 0.01$) compared with baseline after sham correction, whereas M1-tbTUS significantly decreased beta power (−15.6 ± 4.2% [−23.9 to −7.3%], $r = -0.32$, $P_{adj} < 0.01$) and increased theta power (8.6 ± 3.4% [1.8 to 15.3%], $r = 0.31$, $P_{adj} < 0.01$) (Fig. 4A, bottom row). In contrast, Occ-tbTUS had no significant effects. The power changes at each specific time point are presented in figs. S1 and S2 and were insignificant across all time points. We also performed between-group comparison using a linear mixed-effects model, which revealed that GPi-tbTUS significantly

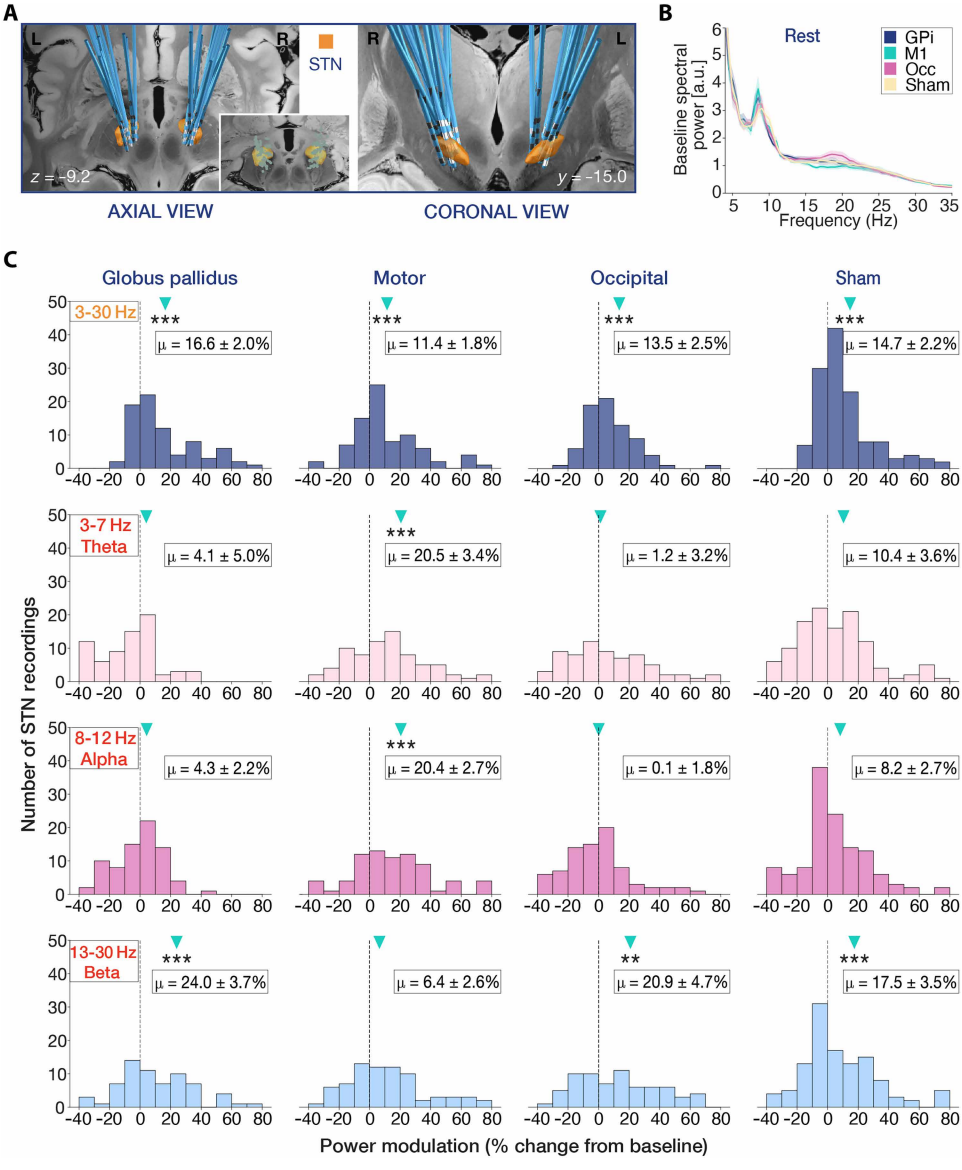

Fig. 3. DBS electrode localization and pooled power changes from baseline for all conditions at rest. (**A**) The DBS lead pairs of 17 patients were visualized in relation to the STN using axial and coronal views. (**B**) Baseline spectral power across the four conditions at rest. a.u., arbitrary units. (**C**) The histograms illustrate the percentage change in spectral power (3 to 30 Hz, 3 to 7 Hz, 8 to 12 Hz, and 13 to 30 Hz from top to bottom rows) relative to baseline for each sonication condition. Green downward-pointing triangles indicate the mean of the distribution, and the vertical dashed line at 0% represents the baseline reference. Data were pooled across all hemispheres ($n = 20$ for GPi, M1, and occipital; $n = 34$ for sham) and across four postbaseline time points (20 × 4 and 34 × 4 recordings in the histograms, respectively). The Kruskal-Wallis test was used to compare baseline power across conditions, and the Wilcoxon signed-rank test with FDR correction was used to assess within-condition changes from baseline. Statistical significance is marked by asterisks (**$P < 0.01$; ***$P < 0.001$).

increased beta-band power compared with M1-tbTUS (estimate = 0.33, $r = 0.6$, $P_{adj} < 0.05$) and Occ-tbTUS (estimate = 0.23, $r = 0.7$, $P_{adj} < 0.05$), whereas the other between-condition differences were not significant (Fig. 4B).

tbTUS of M1 modulates power differently during movement and rest

During finger tapping, we found no statistically significant differences in baseline spectral power across the four conditions in the theta (3 to 7 Hz, $P = 0.79$), alpha (8 to 12 Hz, $P = 0.30$), and beta (13 to 30 Hz, $P = 0.04$) bands (Kruskal-Wallis test), with all post hoc comparisons yielding nonsignificant adjusted P values (Fig. 5A). We assessed baseline power during movement and at rest using within-visit paired measurements ($n = 47$ visits), pairing each patient's movement baseline with their corresponding rest baseline, and found that the overall power (3 to 30 Hz) significantly decreased during movement compared with during rest (1.55 ± 0.01 → 1.49 ± 0.01, $P_{adj} < 0.001$). Band-specific analysis revealed that movement significantly increased theta band power compared with rest (3.57 ± 0.11 → 3.65 ± 0.1, $P_{adj} < 0.001$), whereas alpha (1.91 ± 0.04 → 1.70 ± 0.03, $P_{adj} < 0.001$) and beta (0.91 ± 0.03 → 0.86 ± 0.03, $P_{adj} < 0.001$) band power significantly decreased (Fig. 5B). When postsonication time points were pooled, all conditions showed a significant power increase in the 3- to 30-Hz range compared with baseline, a pattern similar to LFP changes at rest (GPi: 29.8 ± 2.3%, $r = 0.87$; M1: 15.2 ± 1.8%, $r = 0.75$; occipital: 21.2 ± 2.8%, $r = 0.77$; sham: 16.7 ± 2.1%, $r = 0.7$; all FDR-adjusted $P < 0.001$). An analysis by frequency band showed that power significantly increased across all three bands in the GPi condition (theta: $r = -0.35$, $P_{adj} < 0.05$; alpha: $r = 0.35$, $P_{adj} < 0.05$; beta: $r = 0.84$, $P_{adj} < 0.001$) and the M1 condition (theta: $r = 0.45$, $P_{adj} < 0.01$; alpha: $r = 0.61$, $P_{adj} < 0.001$; beta: $r = 0.36$, $P_{adj} < 0.01$). In contrast, the occipital condition exhibited a significant change only in the beta band (theta: $r = 0.12$, $P_{adj} = 0.35$; alpha: $r = 0.07$, $P_{adj} = 0.58$; beta: $r = 0.56$, $P_{adj} < 0.001$), whereas the sham condition showed significant changes in the theta ($r = 0.26$, $P_{adj} < 0.05$) and beta ($r = 0.53$, $P_{adj} < 0.001$) bands but not in the alpha band ($r = 0.17$, $P_{adj} = 0.12$) (Fig. 5C). Paired sham-corrected power in the GPi group during movement showed a significant decrease in theta power (−10.4 ± 4.5 [−19.2 to −1.7]%, $r = -0.41$, $P_{adj} < 0.01$) and an increase in beta power (26.8 ± 4.8 [17.4 to 36.1]%, $r = 0.58$, $P_{adj} < 0.001$), whereas the M1 group exhibited a significant increase only in the alpha band (13.3 ± 4.0 [5.4 to 21.2]%, $r = 0.41$, $P_{adj} < 0.01$). No significant changes were observed in the occipital group across all three frequency bands (Fig. 5D). We then compared power changes between rest and movement, finding

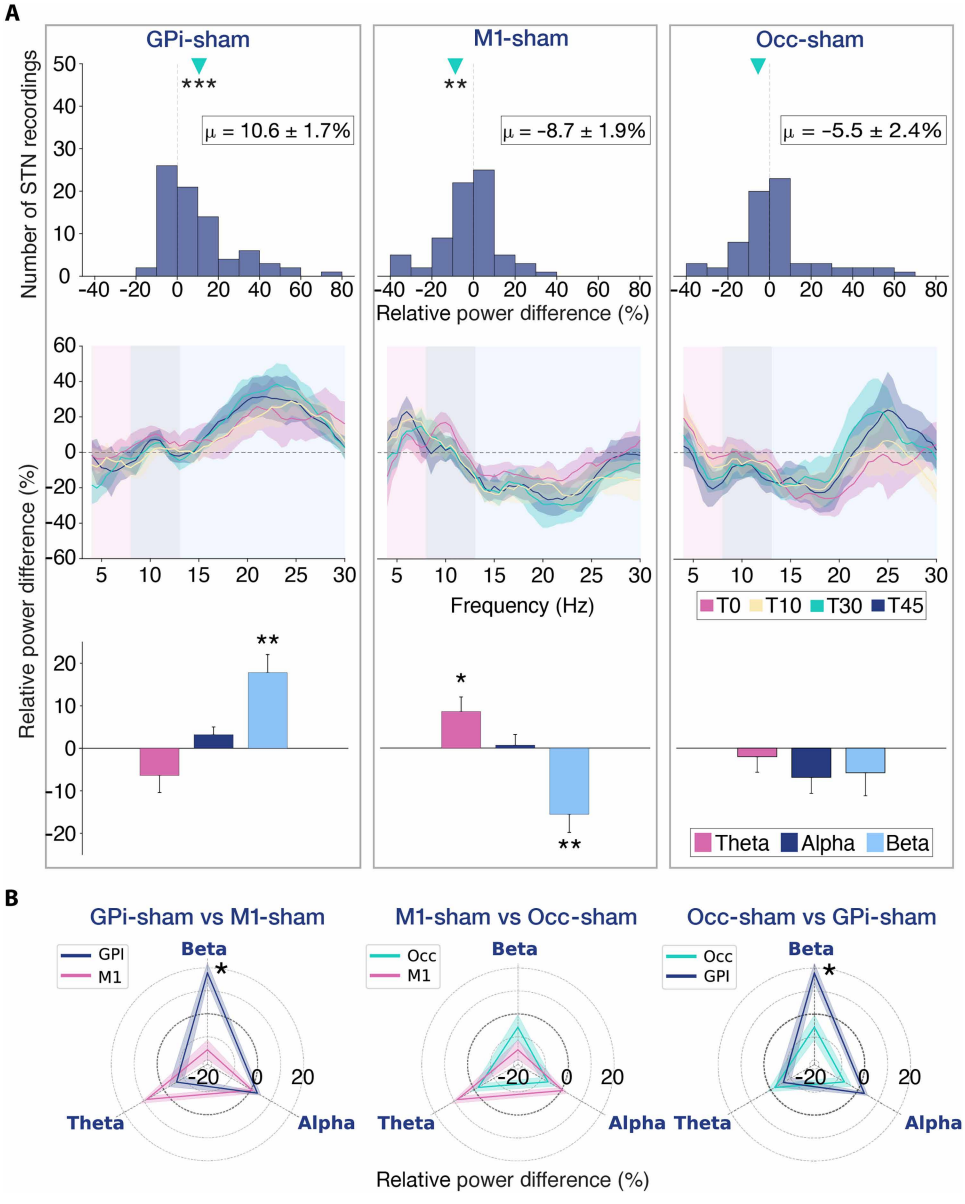

Fig. 4. Sham-corrected percent power change from baseline across tbTUS conditions at rest. (**A**) Top row: Histograms illustrate the differences in power change (3 to 30 Hz) between active tbTUS conditions and their paired sham. Green downward-pointing triangles indicate the mean of the distribution, and the vertical dashed line at 0% represents the baseline reference. Middle row: Percent power changes from baseline across frequency are shown separately for all four post-baseline time points. The mean spectral power difference was smoothed using a moving average filter with a window size of 5. Bottom row: Bar plots show the sham-corrected mean percent changes in power from baseline within the theta, alpha, and beta frequency bands, pooled across all post-baseline time points for each active tbTUS condition. (**B**) Comparative analysis of sham-corrected power changes across active sonication conditions. Error bars and shaded regions represent SEM [in the middle row of (A); the SEM was scaled by a factor of 1.5 to enhance visual differentiation between tightly overlapping lines]. The Wilcoxon signed-rank test with FDR correction was used for within-subject sham-corrected comparisons, and between-active-condition comparisons were derived from linear mixed-effects models fitted separately for each frequency band with FDR correction. $n = 80$ recordings per active condition. Statistical significance is marked by asterisks (*$P < 0.05$; **$P < 0.01$; ***$P < 0.001$).

that the increase in alpha power in the M1-tbTUS condition was significantly more pronounced during movement than at rest ($r = 0.38$, $P_{adj} < 0.05$), whereas all other comparisons were nonsignificant (Fig. 5D).

Differential beta burst duration changes across tbTUS conditions

A representative 10-s LFP recording from participant 1 during the sonication time point of a sham condition visit is shown in Fig. 6A, illustrating the method used to compute beta burst duration. The change in beta burst duration showed a significant increase only in the occipital (6.6 ± 2.6%, $r = 0.38$, $P_{adj} < 0.05$) and sham (9.2 ± 3.3 [2.5 to 15.8]%, $r = 0.29$, $P_{adj} < 0.05$) groups. In the M1 group, beta burst duration decreased (−4.1 ± 1.8%, Cohen's $d = -0.36$, $P < 0.05$), but this effect did not remain significant after multiple comparisons correction ($P_{adj} = 0.058$). No significant change from baseline was observed in the GPi group (−0.2 ± 2.5%, $r = -0.07$, $P_{adj} = 0.73$) (Fig. 6B). Pairwise comparisons analysis revealed a significant difference between M1 and sham ($r = -0.26$, $P_{adj} < 0.05$) and between M1 and occipital ($r = -0.34$, $P_{adj} < 0.05$) stimulation (Fig. 6C). As an exploratory analysis, we assessed STN coherence and found no within-hemisphere changes in any band, whereas between hemispheres only M1-tbTUS increased beta coherence (no theta/alpha effects and no effects for GPi-tbTUS or Occ-tbTUS) (see fig. S3 for details).

Clinical effects of tbTUS

We assessed MDS-UPDRS-III scores for each patient immediately before baseline recordings and immediately after the final recordings, with video assessments scored in a blinded manner. Three sessions (3 of 47, 6.4%) were excluded from the MDS-UPDRS-III analysis after sensitivity testing (see the Statistical analysis section for details). The M1 group showed significant improvement [42.8 ± 21.0 → 38.2 ± 20.7, $n = 9$, paired $t(8) = 2.4$, $d = -0.8$, $P < 0.05$], whereas no significant changes were observed in the other groups [GPi: 39 ± 14 → 39.9 ± 16.3, $n = 9$, paired $t(8) = -0.41$, $d = 0.14$, $P = 0.69$; Occ: 39 ± 16.5 → 39.8 ± 12.9, $n = 9$, paired $t(8) = -0.28$, $d = 0.09$, $P = 0.78$; sham: 42.1 ± 16.6 → 43.9 ± 17.8, $n = 17$, paired $t(16) = -1.13$, $d = 0.27$, $P = 0.28$] (Fig. 7A). Using the full (non–outlier-excluded) dataset ($n = 10$ paired), the M1 effect became nonsignificant [$t(9) = -0.08$, $P = 0.94$], whereas GPi ($P = 0.32$) and occipital stimulation ($P = 0.56$) likewise remained nonsignificant. MDS-UPDRS-III score changes in the five sessions where patients

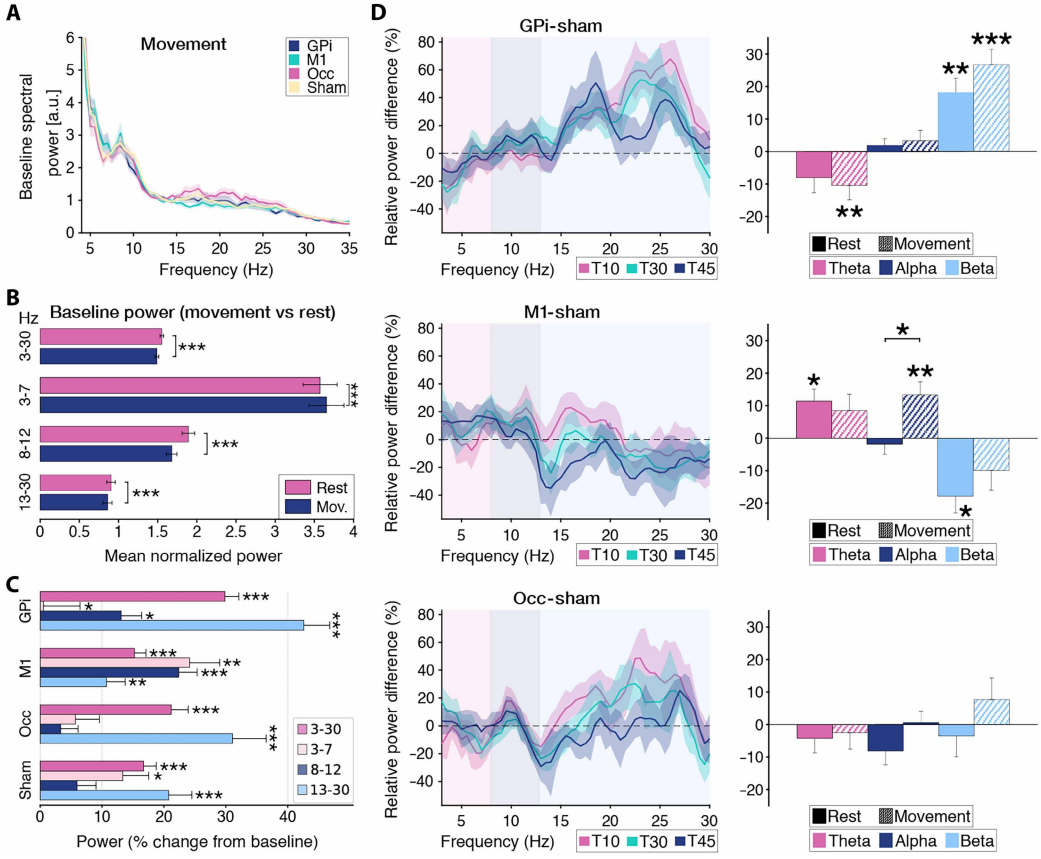

Fig. 5. tbTUS-induced changes in spectral power during movement. (**A**) Baseline spectral power during movement (Kruskal-Wallis, post hoc Mann-Whitney *U*, FDR-adjusted). (**B**) Band-specific analysis of baseline power during movement and at rest (pooled across 47 visits and both hemispheres) (Wilcoxon signed-rank, FDR-adjusted). Error bars represent ±SEM. (**C**) Bar plots show the percent change in spectral power relative to baseline across four frequency bands—broadband (3 to 30 Hz), theta (3 to 7 Hz), alpha (8 to 12 Hz), and beta (13 to 30 Hz)—for each sonication condition. Values were pooled across hemispheres ($n = 20$ for GPi, M1, and occipital; $n = 34$ for sham) and across three postbaseline time points ($n = 20 \times 3$ and 34×3 recordings, Wilcoxon signed-rank, FDR-adjusted). Error bars reflect the SEM in the positive direction only. (**D**) Left column: Frequency-resolved power differences between active and paired sham conditions during movement, across postsonication time points. Right: Paired sham-corrected mean percent power changes from baseline in theta, alpha, and beta bands, pooled across postsonication time points, during rest and movement. Statistical comparisons were performed within each state and between corresponding bands across rest and movement ($n = 60$ recordings per band per condition; 10 patients x 2 hemispheres x 3 time points, noting that the T0 time point lacked a movement task) using Wilcoxon signed-rank tests with FDR correction. $^{*}P < 0.05$; $^{**}P < 0.01$; $^{***}P < 0.001$.

reported subjective improvement (-3.2 ± 6.6, $n = 5$) were not statistically different from those in other sessions ($+0.5 \pm 7.0$, $n = 39$; Mann-Whitney $U = 68.5$, $P = 0.29$). We examined whether beta-band power correlated with MDS-UPDRS-III scores in the M1 group. We found a positive correlation between baseline MDS-UPDRS-III scores and baseline beta-band LFP power ($r = 0.76$, $P_{adj} < 0.05$), as well as between postvisit MDS-UPDRS-III scores and beta-band LFP power at the T45 time point ($r = 0.67$, $P_{adj} < 0.05$, $n = 9$, paired) (Fig. 7B, left column). Subsequently, we assessed the correlation between MDS-UPDRS-III percentage change and sham-corrected beta power change from baseline in the M1 group at T45 but found no significant correlation ($r = 0.49$, $P_{adj} = 0.18$; Fig. 7B, top right). Similarly, pooling data across all postsonication time points (T0 + T10 + T30 + T45) did not alter the results ($r = 0.55$, $P_{adj} = 0.18$, $n = 9$, paired; Fig. 7B, bottom right). Changes in accelerometer-recorded finger-tapping velocity were not significant across all conditions [sham $n = 17$: $F_{Fisher}(2.21,35.3) = 1.40$, $P = 0.26$; M1 $n = 10$: $F_{Fisher}(2.61,23.5) = 0.29$, $P = 0.8$; GPi $n = 10$: $F_{Fisher}(2.37,21.3) = 0.4$, $P = 0.71$; Occ $n = 10$: $F_{Fisher}(2.02,18.16) = 0.53$, $P = 0.6$] (Fig. 7C).

DISCUSSION

We investigated the effects of individualized TUS targeting both cortical and subcortical hubs of the motor network by direct recording of STN LFPs and evaluated clinical outcomes in patients with PD. We found that the effects of tbTUS were both target specific and frequency band specific: Compared with the sham condition, M1-tbTUS decreased beta activity and increased theta activity, GPi-tbTUS increased beta activity, and Occ-tbTUS had no significant effect. The modulation was also brain state dependent given that M1-tbTUS produced different effects during movement versus rest. Beta burst duration increased during sham and occipital stimulation but remained stable during M1-tbTUS, the only condition differing significantly from both and showing a modest improvement in MDS-UPDRS III scores.

PD exhibits diverse clinical presentations, with distinct LFP features differentiating akinetic-rigid (AR) and tremor-dominant (TD) subtypes (*39*, *40*). However, our cohort was less affected by this heterogeneity because nearly all of our patients were late-stage AR or equivalent type, with only one exception (Table 1). Their baseline LFP

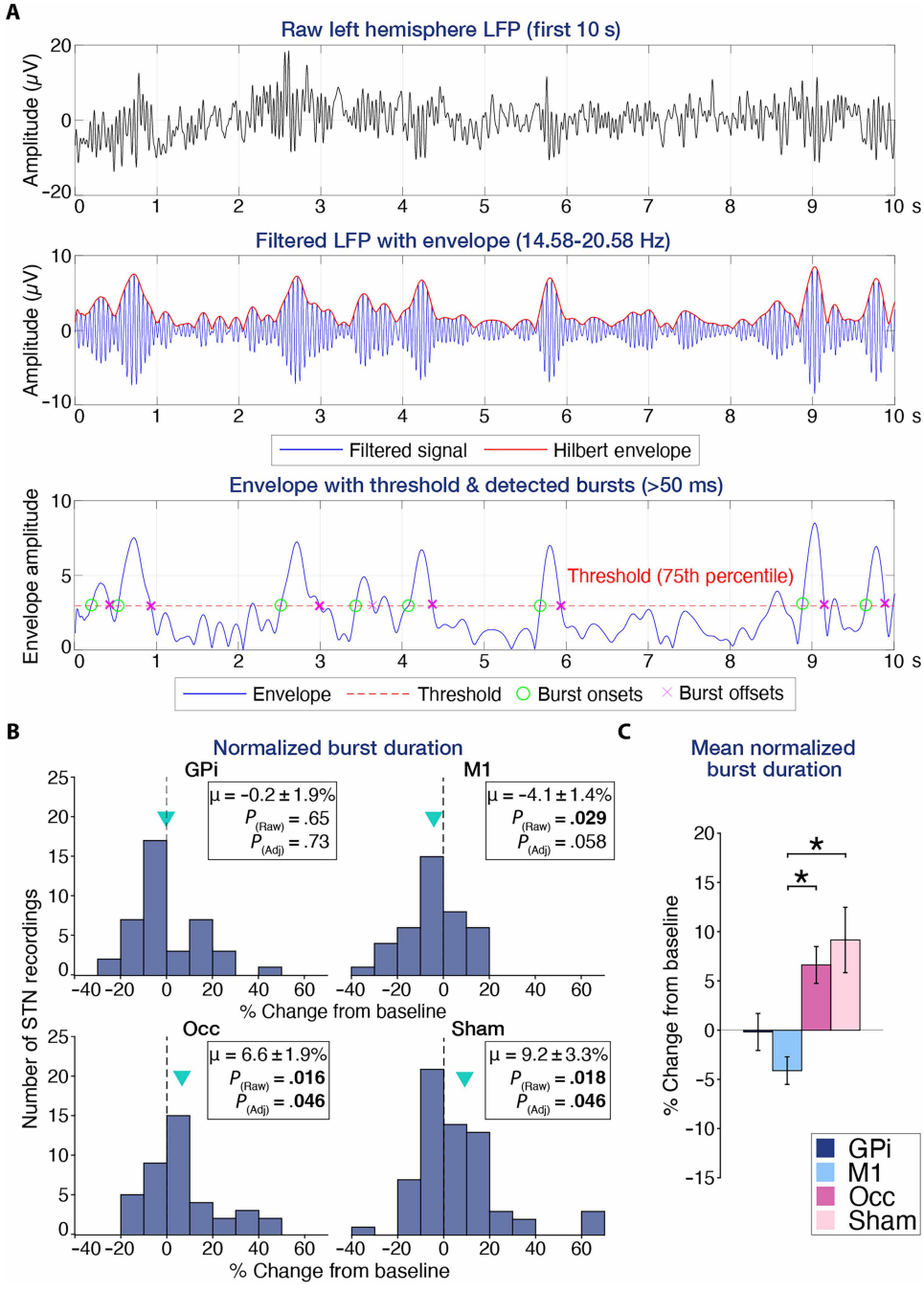

Fig. 6. tbTUS-induced changes in beta burst duration. (**A**) Beta bursts in the raw LFP signal (top row) were identified by first applying a fourth-order Butterworth band-pass filter centered on each participant's peak beta frequency, determined using Welch's method with a 2-s Hanning window (middle row). A ±3-Hz range around the peak was selected, ensuring a minimum bandwidth of 6 Hz. The filtered signal was then processed using the Hilbert transform to extract its analytic envelope, which reflects the instantaneous amplitude of beta oscillations. Bursts were defined as periods during which the envelope exceeded the 75th percentile threshold of the entire signal (bottom row). Onset and offset were marked at threshold crossings, and only events lasting at least 50 ms were included in the final analysis. (**B**) Histograms show the distribution of normalized changes in mean beta burst duration across postbaseline recordings for each condition. For each recording, mean burst duration was calculated and normalized to baseline as (postbaseline − baseline)/baseline; values were then pooled across the four postbaseline time points. The *y* axis indicates the number of STN recordings in each bin, and green downward-pointing triangles denote the mean percent change from baseline (Wilcoxon signed-rank/paired *t* test, FDR-adjusted; $n = 10$ active and $n = 17$ sham). (**C**) Pairwise comparison of the mean normalized burst duration change (Mann-Whitney *U*, FDR-adjusted). Error bars represent ±SEM. $^*P < 0.05$.

spectral power in the ON-medication condition exhibited similar characteristics, with suppressed beta activity and an alpha peak, a feature often observed in patients with chronic DBS after several months of stimulation (*41*, *42*). We observed an increase in LFP power (3 to 30 Hz) across all three active tbTUS conditions. Although this could suggest a nonspecific neuromodulatory effect of tbTUS, a similar power increase in the sham condition indicates that the results were likely confounded by levodopa wear-off. This interpretation aligns with the study timeline, where patients received levodopa 45 to 75 min before baseline recordings, coinciding with its peak effect. The subsequent gradual loss of efficacy and corresponding power increase are consistent with expected pharmacokinetic dynamics of levodopa (*43*). A sub-band analysis revealed that, although 3- to 30-Hz power increased across all conditions, the patterns differed between sonication targets. M1 sonication increased the low-frequency range (theta and alpha) without affecting beta, whereas the other conditions increased beta with no impact on low-frequency activity. This demonstrated region-specific and frequency-specific effects of tbTUS in our study. The spatial sensitivity of TUS has been previously demonstrated, showing that shifting the sonication focus by even a centimeter can produce different effects (*44*). Consistent with these findings, our study further confirms that targeting different brain regions with the same TUS parameters results in distinct modulatory effects on different frequency bands at the same recording site, the STN, reinforcing our understanding of spatial specificity. This could be especially important for future studies aiming to probe brain function using TUS.

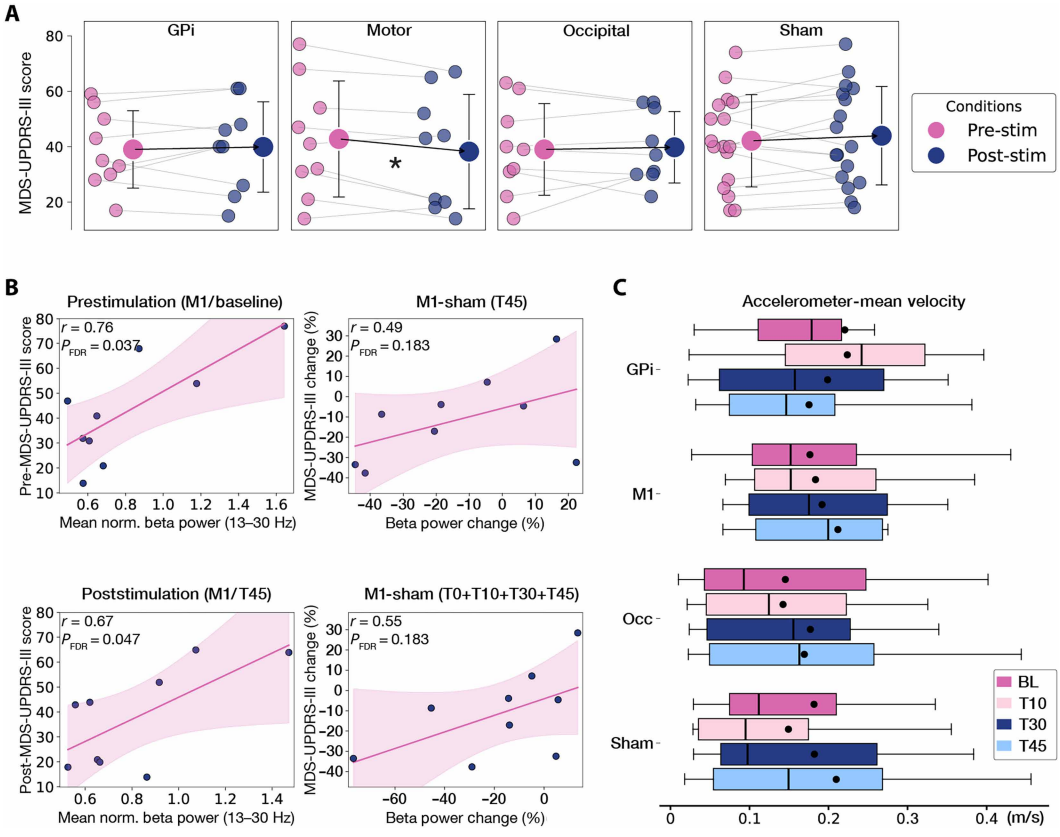

Fig. 7. tbTUS effects on clinical scores. (**A**) Pre- and poststimulation mean MDS-UPDRS-III scores were compared separately for the GPi, M1, occipital, and sham conditions (paired Student's *t* test; $n = 9$ active and $n = 17$ sham). Small dots represent individuals, large dots represent means, and error bars indicate ±SD. $^*P < 0.05$. (**B**) Scatterplots show the relationship between the mean normalized beta power (13 to 30 Hz) and MDS-UPDRS-III scores in the M1 group. Baseline beta power is plotted against presonication MDS-UPDRS-III scores (top left), and beta power at T45 is plotted against postsonication MDS-UPDRS-III scores (bottom left). Sham-corrected changes in beta power relative to baseline are plotted against changes in MDS-UPDRS-III scores, using beta power change between T45 and baseline (top right) and beta power change pooled across T0, T10, T30, and T45 relative to baseline (bottom right) (Pearson correlation, FDR-adjusted; $n = 9$). The solid line indicates the linear regression fit; the shaded area represents the 95% confidence interval. (**C**) Box plots show accelerometer-recorded finger-tapping velocity across conditions (repeated-measures ANOVA; $n = 10$ active, $n = 17$ sham). Boxes indicate the interquartile range (IQR) with the median shown as a line; whiskers extend to 1.5 × IQR; dots indicate the mean.

To minimize the influence of confounding factors such as levodopa wear-off, experimental setup, anxiety, and placebo effects, we subtracted each patient's sham condition from their active conditions to isolate the true effect of tbTUS. The results indicated that M1-tbTUS decreased beta power and increased theta power, whereas GPi-tbTUS increased beta power. In contrast, Occ-tbTUS showed no significant effect. We chose to sonicate the middle occipital gyrus because it lacks a direct structural connection to the STN (*45*) and is functionally a component of an alpha rhythm-dominant network (*46*). This contrasts with the motor cortex, which exhibits beta oscillatory activity at rest and connects with the basal ganglia through a dopamine-modulated whole-brain network (*46*).

Increased STN beta activity is associated with parkinsonian signs such as rigidity and bradykinesia and is suppressed by levodopa or DBS (*39*, *47*). M1-tbTUS reduced beta activity and enhanced theta power—an oscillatory shift associated with improved symptom control in PD. Repetitive transcranial magnetic stimulation (rTMS) studies have shown that high-frequency stimulation of M1 is excitatory and leads to clinical improvements in bradykinesia and rigidity (*48*, *49*). M1-tbTUS may exert effects through a comparable mechanism by modulation of cortical excitability in PD (*33*). This is consistent with our previous studies showing that tbTUS targeting M1 enhances cortical excitability, as measured by TMS, in both healthy individuals (*24*, *50*, *51*) and patients with PD (*37*, *52*). Although increased motor cortical excitability with intermittent tbTUS was replicated in rodents (*53*), it has not been successfully reproduced in humans by an independent group (*54*). Nonetheless, several other studies have demonstrated distinct neuromodulatory effects of tbTUS at various targets in humans (*55*–*58*). A recent study demonstrated that tbTUS applied to the posterior cingulate selectively reduced γ-aminobutyric acid (GABA) concentrations (*57*), aligning with the excitatory effect of tbTUS observed in this study. In contrast, the up-regulation of beta activity by GPi-tbTUS could represent modulation in an undesired direction in PD. The opposing effect of GPi-tbTUS compared with high-frequency GPi-DBS—which functions as an inhibitory lesion through depolarization block—suggests that tbTUS exerts an overall excitatory influence on the GPi. Although the observed changes appeared excitatory, this should not be taken as evidence that TUS directly evokes action potentials. Rather, the prolonged time course of the effect—supported

by our pooled analysis of online and offline data, with the latter extending up to 50 min postsonication—indicates a shift in neural circuit excitability. We recorded over this extended window because TUS mechanisms involving mechanical membrane interactions, mechanosensitive ion channels, and astrocytic signaling—processes known to support plasticity and metaplasticity—make sustained postsonication effects physiologically plausible and increasingly supported by recent studies (*24*, *25*, *57*, *59*–*61*).

We demonstrated that movement (finger tapping) reduced alpha and beta power and increased theta activity before tbTUS application, resulting in a shift toward a low-frequency–dominant state—consistent with previous findings (*62*). We observed distinct neuromodulatory effects of M1-tbTUS during movement compared with the resting state. Although sham-corrected M1-tbTUS during movement continued to show reduced beta and increased theta activity—similar to its effects at rest—these changes were no longer statistically significant during movement. This loss of effect may reflect a ceiling effect given that both movement and tbTUS appear to shift neural activity toward lower frequencies—specifically driving beta power into the theta range—which may limit the additional modulatory impact of tbTUS during movement. The increased alpha power observed with M1-tbTUS during movement may indicate compensatory engagement of alternative oscillatory pathways, potentially reflecting an adaptive shift when theta modulation has reached saturation because of the combined effects of movement and stimulation. In contrast, the effect of GPi-tbTUS was more pronounced during movement, with a stronger enhancement of beta activity and a reduction in theta power. This brain state–dependent effect of TUS is consistent with several preclinical studies, and the current findings provide additional evidence supporting this phenomenon (*21*, *28*–*32*).

Beta burst duration has been associated with motor symptom severity in PD (*63*). In our study, the increases in beta burst duration observed during sham and occipital stimulation were most likely driven by time-dependent factors such as gradual levodopa wear-off. In contrast, M1-tbTUS may have counteracted these nonspecific increases, resulting in a relative stabilization of beta dynamics. Although GPi-tbTUS enhanced overall beta activity, it did not increase beta burst duration, suggesting a dissociation between beta power and burst dynamics.

We assessed motor outcomes using two complementary approaches: (i) clinician-rated MDS-UPDRS-III scores and (ii) accelerometer-based measurements of finger-tapping velocity. MDS-UPDRS-III scores were assessed in a double-blind manner: One blinded neurologist conducted and video recorded the examinations, whereas a second blinded neurologist evaluated the anonymized videos. This approach eliminates interrater variability; any unavoidable intrarater fluctuations that remain are random in nature and evenly distributed across conditions. The MDS-UPDRS-III scores showed a positive correlation with absolute beta power both before and after sonication, consistent with findings reported (*39*). M1-tbTUS was the only condition that produced a significant improvement in MDS-UPDRS-III scores, with a mean change of 4.5 points. Although smaller than the typical effects observed with DBS, this improvement exceeds the minimal clinically important difference of −3.25 points, indicating clinical relevance (*64*). The absence of a similar improvement in parkinsonian signs with M1-tbTUS in our prior studies likely stems from differences across studies in patient cohorts, medication state, sonication characteristics and delivery approaches, as well as variations in clinical rating procedures (*37*, *52*, *65*). Nevertheless, the clinical improvement observed with M1-tbTUS in the present study should be interpreted with caution because of several uncertainties: (i) The sample size was relatively small ($n = 9$), raising the possibility of a false-positive finding; (ii) no statistically significant improvement was observed in accelerometer-recorded movement velocities; (iii) although MDS-UPDRS-III scores correlate with absolute beta power, changes in beta power did not correlate with changes in MDS-UPDRS-III scores; and (iv) GPi sonication led to an increase in beta power without a corresponding increase in MDS-UPDRS-III scores. Although beta power is a key biomarker of motor symptoms, it is not the sole factor; clinical dynamics are multifaceted, and other metrics, such as beta burst duration, may also play important roles. These uncertainties highlight the need for multidimensional evaluation using a combination of outcome measures, including clinical scores, and complementary neurophysiological tools, such as LFPs and accelerometry, particularly in early-stage experimental studies where the risk of false hope remains high.

Our study has limitations. During GPi sonication, neighboring structures such as the globus pallidus externus and internal capsule may have been partially affected, potentially contributing to the observed effects. Similarly, M1 sonication likely affected not only cortical gray matter but also underlying white matter fibers. Extensive modeling in our study, incorporating skull distortion calculations, final target and trajectory corrections, and the use of neuronavigation systems, may contribute to improved targeting accuracy. However, the actual error margin of TUS delivery and potential off-target sonication remains uncertain given that these are only predictive models. The field still requires robust evidence, using direct methods such as MR-ARFI, to precisely determine the spatial error margin of TUS delivery (*66*). In addition, the use of dedicated head-stabilization or transducer-holder systems such as custom stereotactic face-and-neck fixation masks (*67*) or 3D-printed mechanical holders with *x-y* axis positioning indicators (*68*, *69*) may further improve targeting accuracy in future studies. Another targeting challenge in this study was that our commercial TUS device, NeuroFUS, has a maximum focal depth of 82 mm, which was insufficient to reach the STN through a vertex approach in some patients. Moreover, a perpendicular trajectory through the temporal bone was often partially obstructed by the ears. For these reasons, we opted to target the GPi instead given that it is larger, more tolerant to minor deviations, and avoids direct sonication at the DBS recording site, thereby minimizing the potential risk of recording artifacts.

The participants in this study had late-stage PD. For patient comfort and study feasibility, they were studied in the ON-medication state. This imposes an important limitation on interpretation of the results because levodopa is known not only to improve motor performance but also to reduce beta oscillations in basal ganglia loops in patients with PD. This limitation prevented us from isolating the pure effect of TUS because dopamine fluctuations from levodopa wear off over time, introducing a confounding variable. To address this, we implemented a sham condition by setting the device to an intensity of 0 W/cm^2 while maintaining continuous auditory masking and replicating all procedural elements, which is an accepted sham technique in the field (*7*). In addition, we used an active sham condition by targeting the Occ to assess whether the observed effects were network specific. Although the area we targeted in the Occ is not a primary motor hub in PD, it may still exert secondary or indirect influences on the motor network through visuomotor, associative, and other integrative cortical pathways. An alternative

sham approach to consider in future studies would be targeting a nonparenchymal intracranial site, such as the lateral ventricles (*70*). ON-medication studies are also inherently confounded by motor fluctuations, which may be large enough to influence clinical scores or occur more subtly across sessions; however, any such effects would be expected to apply uniformly across sessions and time points and therefore introduce random variability rather than systematic bias toward any specific active condition. A similar source of noise arises from the DBS-OFF state: The 30-min washout used here accounts for about 75% of the clinical return toward the OFF-DBS baseline, whereas the remaining 25% recovers gradually during the testing period, as shown in prior DBS washout studies. Because this residual improvement elevates the baseline clinical score and decays over time, any true tbTUS-related clinical effect would be expected to be modestly underestimated rather than exaggerated. In addition, not all participants completed every stimulation condition, which reduced full within-subject control and may introduce additional interindividual variability. To mitigate this to some extent, linear mixed-effects models with subject-level random effects were used where appropriate to accommodate repeated measures and unequal condition sampling.

Baseline analyses in our study confirmed that, in the ON-medication state, STN beta-band power is already suppressed and UPDRS motor scores are comparatively better than in the OFF-medication condition. This favorable physiological and clinical baseline leaves little room for additional beta power reduction or substantial further UPDRS improvement. Consequently, any incremental effects of TUS in the ON-medication state are likely to be small and difficult to detect because of a possible ceiling effect. In patients with dyskinesias in the ON-medication state, a narrow-band, finely tuned gamma oscillation centered around ~70 Hz may be present and correlate with dyskinesia severity (*71*). However, because of the limited number of patients with dyskinesias in our cohort (5 of 19), group-level analysis of tbTUS effects on finely tuned gamma was not feasible.

Our study presented a method for directly monitoring circuit activity with high spatiotemporal resolution using LFPs to evaluate TUS effects, offering a translationally relevant approach that could inform future applications across DBS-treated conditions such as depression, addiction, Alzheimer's disease, epilepsy, and other psychiatric disorders. For this TUS-LFP method to be widely adopted across centers, it will be important to show that it can be replicated using other ultrasound neuromodulation platforms. The NeuroFUS system used here was a four-element, handheld device with advantages of technical simplicity, portability, and fixed factory calibration. In contrast, large phased-array systems with hundreds of elements pose unique safety considerations because interactions between multiple beams and implanted DBS hardware may differ from those of simpler handheld systems. These effects should be verified through site-specific phantom testing for the intended parameters, as we did for this study (*35*), particularly for MR-guided systems such as Insightec, where the combined magnetic and acoustic fields add further complexity.

Cavitation remains an important safety consideration in ultrasound-based interventions because it can cause tissue damage if uncontrolled (*72*). In patients in the postoperative period, even small air pockets along electrode trajectories can act as cavitation nuclei; therefore, updated neuroimaging should be obtained to confirm the absence of air before sonication, and waiting at least 1 to 2 months after DBS surgery is advisable before any TUS intervention. Currently, no formal safety guidelines exist specifically for focused ultrasound neuromodulation. The ITRUSST consensus on biological safety proposed that an MI not exceeding 1.9 is associated with nonsignificant risk (*38*). However, MI values within the nonsignificant risk range do not necessarily ensure safety in patient populations given that mechanical safety depends not only on acoustic amplitude but also on pulse characteristics, monitoring strategies, and patient-specific factors. Conversely, higher MI values may be tolerated in well-characterized and carefully monitored settings, underscoring that safety in patient populations is context dependent (*73*). Beyond safety, future work should also focus on acquiring higher-resolution and multimodal data to better characterize TUS mechanisms. Electrocorticography (ECoG) recordings from patients with DBS implants enrolled in adaptive DBS trials may provide clearer signals than LFPs and yield more mechanistic insights (*74*). Similarly, combining TUS with MR spectroscopy or functional MRI could help link electrophysiological changes to metabolic and network-level responses (*57*, *58*, *67*, *75*–*77*).

Future directions for PD research may involve testing inhibitory TUS protocols in basal ganglia structures. On the other hand, excitatory protocols might still hold potential for targets such as the pedunculopontine nucleus, although its small size and deep location make it difficult to target without off-target effects. Another strategy could involve adjusting the intensity and duration of M1-tbTUS to enhance its effect size. Accelerated protocols involving multiple sessions per day over several weeks—similar to those used in TMS studies for depression and obsessive-compulsive disorder (*78*, *79*)—should be explored with TUS to achieve more sustained benefits. For cortical areas such as M1, the effects of TUS should be compared to other established noninvasive brain stimulation methods such as rTMS. Beyond its application in PD, TUS may have therapeutic potential for pain management. A recent study demonstrated pain reduction in healthy participants after inhibitory TUS targeting the dorsal anterior cingulate cortex (*80*). Excitatory protocols such as tbTUS could be explored as a potential treatment for neuropathic pain, given that low-frequency DBS of the periventricular gray has shown clinical efficacy under such conditions (*81*).

MATERIALS AND METHODS

Study design

The objective of this prospective randomized study was to determine whether TUS applied to different brain regions modulates STN LFPs in patients with PD and whether such target-dependent electrophysiological changes are associated with clinical effects. The primary outcome was the change in postsonication LFP power relative to baseline, and the difference in this change between active and sham stimulation conditions. The study included four distinct sonication conditions: (i) passive sham (I_{sppa} set to 0 W/cm^2); (ii) active sham (sonication of a nonmotor cortical region, the Occ); (iii) active M1 (sonication of the primary motor cortex); and (iv) active GPi (sonication of the GPi). All participants ($n = 17$) underwent a passive sham condition in a single session, along with one active condition in a separate session spaced at least 1 week apart. The at least 1-week washout interval was chosen on the basis of our previous experiment in patients with PD, in which motor cortex excitability measured by TMS returned to baseline values within 1 hour after a single sonication session (*52*). The order of the active and sham sessions was randomized. Each active condition was designed to include 10 participants, with a total of 30 active sessions randomized and assigned to new participants as they joined the study. Data collection concluded once

this predefined number of sessions was reached. After completing one active and one sham session, participants were invited to participate in a third session involving another active condition [$n = 13/17$, 76% agreed; reasons for declining included long travel distance to a hospital (two in M1 and one in the occipital group) and difficulty tolerating symptom severity during the DBS-OFF condition (one in M1)]. Those who agreed were assigned to a new active condition based on the randomization chart. Participants remained blind to the sonication conditions until they completed all visits. The inclusion criteria included patients with PD of any age, sex, and severity who were stable on dopaminergic medications and had undergone bilateral STN-DBS with a commercial IPG capable of both stimulation and recording (Percept PC, Medtronic, Dublin, Ireland), encompassing both newly implanted DBS systems and older systems upgraded with a Percept PC battery replacement. Exclusion criteria were (i) neurological conditions other than PD; (ii) major psychiatric disorders; (iii) Montreal Cognitive Assessment (MoCA) score < 22; (iv) cardiac and other neurological implants; (v) history of intracranial lesioning and implantation of more than 2 leads in a single patient; (vi) major illness, infection, or pregnancy; and (vii) damaged lead contacts. Seventeen patients were recruited for the study, with informed consent obtained from each participant. The sample size was not predetermined using any statistical method. Patient characteristics are given in Table 1. The details of the DBS procedure have been described previously (*82*). This study was approved by the Research Ethics Board of the University Health Network, Canada (protocol no. 18-5082), adhered to the latest version of the Declaration of Helsinki, and was preregistered on ClinicalTrials.gov under the identifier NCT05965960.

Statistical analysis

The presentation of continuous variables involves reporting the means ± SD, whereas categorical variables are presented in terms of frequency (percentage). Blinding effectiveness was assessed using binomial tests comparing the proportion of correct guesses against chance level (50%) for each condition. An additional binomial test was performed on the overall distribution of "active" versus "sham" guesses to determine whether participants showed a systematic bias toward one response type, regardless of correctness. Normality was assessed using the Shapiro-Wilk or the Lilliefors test to inform the choice of statistical tests. For paired within-subject comparisons (Figs. 5, B and D, right, and 7A), paired *t* tests or Wilcoxon signed-rank tests were used with FDR correction for LFP analyses. For within-subject/time analyses (Fig. 7C), we used repeated-measures analysis of variance (ANOVA) with Greenhouse-Geisser sphericity correction. Between-subject comparisons (subjective improvement analysis) were performed using the Mann-Whitney *U* test. For comparisons involving mixed paired and unpaired data, a linear mixed-effects model was used to account for within-subject correlations while retaining all available observations. Condition (GPi, M1, and Occ) was modeled as a fixed effect and subject as a random intercept. For the between-active-condition LFP power analyses, sham-corrected power was averaged per participant for each frequency band (theta, alpha, and beta), and a separate model was fitted per band. For acoustic and thermal parameters (I_{SPPA}; MI; and temperature in the brain, skull, and skin), separate models were likewise fitted per parameter. In all cases, between-condition effects were assessed using pairwise mixed-effects comparisons (GPi-M1, Occ-M1, and Occ-GPi); within each band or parameter, these three tests were treated as a single test family ($m = 3$) and adjusted using FDR correction. Models were fit using restricted maximum likelihood estimation. The number of participants contributing paired sessions was $n = 4$ for GPi-M1, $n = 6$ for Occ-GPi, and $n = 3$ for M1-Occ comparisons. A sensitivity analysis was conducted on the MDS-UPDRS-III scores, excluding three sessions with an arbitrary ≥20 points change from baseline because these likely reflected unintended medication status shifts between assessments (motor fluctuations such as wearing-off, ON-OFF phenomena, or delayed ON), which can occur when levodopa doses optimized for the DBS-ON state become suboptimal during DBS-OFF and further amplified by impaired dopamine transport and storage in advanced PD. The excluded sessions were patient 017, GPi (35 > 57); patient 01, M1 (16 > 56); and patient 017, occipital (60 > 29). After identifying outliers in the MDS-UPDRS-III analysis, we assessed the corresponding LFP recordings for outlier behavior. All three fell within the expected variability range and were therefore retained in the main LFP analyses. We conducted Pearson (for linear) or Spearman (for nonlinear) correlation analysis to assess the relationship between LFP recordings and clinical outcomes, reporting the correlation coefficient (r) and adjusted P value. We prespecified two hypothesis families: (A) absolute associations (pre- and post-UPDRS versus corresponding β power) and (B) change-change associations [ΔUPDRS versus Δpooled β and ΔT40 β (sham-corrected)]. Analyses used paired data ($n = 9$), and the FDR was controlled within each family ($m = 2$). All tests were two-sided and considered statistically significant at $P < 0.05$ ($\alpha = 0.05$), and the analyses were performed using R Studio (v2023.12.1+402).

Supplementary Materials

The PDF file includes:
Materials and Methods
Figs. S1 to S3
Tables S1 to S3
References (*83*–*96*)

Other Supplementary Material for this manuscript includes the following:
Data file S1
MDAR Reproducibility Checklist

REFERENCES AND NOTES

1. B. Davidson, A. Bhattacharya, C. Sarica, G. Darmani, N. Raies, R. Chen, A. M. Lozano, Neuromodulation techniques—From non-invasive brain stimulation to deep brain stimulation. *Neurotherapeutics* **21**, e00330 (2024).
2. C. Sarica, C. R. Conner, K. Yamamoto, A. Yang, J. Germann, M. M. Lannon, N. Samuel, M. Colditz, B. Santyr, C. T. Chow, C. Iorio-Morin, D. H. Aguirre-Padilla, S. T. Lang, A. Vetkas, C. Cheyuo, A. Loh, G. Darmani, O. Flouty, V. Milano, M. Paff, M. Hodaie, S. K. Kalia, R. P. Munhoz, A. Fasano, A. M. Lozano, Trends and disparities in deep brain stimulation utilization in the United States: A nationwide inpatient sample analysis from 1993 to 2017. *Lancet Reg. Health Am.* **26**, 100599 (2023).
3. C. Sarica, J.-F. Nankoo, A. Fomenko, T. C. Grippe, K. Yamamoto, N. Samuel, V. Milano, A. Vetkas, G. Darmani, M. N. Cizmeci, A. M. Lozano, R. Chen, Human studies of transcranial ultrasound neuromodulation: A systematic review of effectiveness and safety. *Brain Stimul.* **15**, 737–746 (2022).
4. B. Krasovitski, V. Frenkel, S. Shoham, E. Kimmel, Intramembrane cavitation as a unifying mechanism for ultrasound-induced bioeffects. *Proc. Natl. Acad. Sci. U.S.A.* **108**, 3258–3263 (2011).
5. K. Murphy, E. Fouragnan, The future of transcranial ultrasound as a precision brain interface. *PLOS Biol.* **22**, e3002884 (2024).
6. G. Darmani, T. O. Bergmann, K. Butts Pauly, C. F. Caskey, L. de Lecea, A. Fomenko, E. Fouragnan, W. Legon, K. R. Murphy, T. Nandi, M. A. Phipps, G. Pinton, H. Ramezanpour, J. Sallet, S. N. Yaakub, S. S. Yoo, R. Chen, Non-invasive transcranial ultrasound stimulation for neuromodulation. *Clin. Neurophysiol.* **135**, 51–73 (2022).

7. W. Legon, A. Strohman, Low-intensity focused ultrasound for human neuromodulation. *Nat. Rev. Methods Primers* **4**, 91 (2024).
8. S. Yoo, D. R. Mittelstein, R. C. Hurt, J. Lacroix, M. G. Shapiro, Focused ultrasound excites cortical neurons via mechanosensitive calcium accumulation and ion channel amplification. *Nat. Commun.* **13**, 493 (2022).
9. J. Kubanek, J. Shi, J. Marsh, D. Chen, C. Deng, J. Cui, Ultrasound modulates ion channel currents. *Sci. Rep.* **6**, 24170 (2016).
10. M. L. Prieto, K. Firouzi, B. T. Khuri-Yakub, M. Maduke, Activation of Piezo1 but not NaV1.2 channels by ultrasound at 43 MHz. *Ultrasound Med. Biol.* **44**, 1217–1232 (2018).
11. B. U. Hoffman, Y. Baba, S. A. Lee, C.-K. Tong, E. E. Konofagou, E. A. Lumpkin, Focused ultrasound excites action potentials in mammalian peripheral neurons in part through the mechanically gated ion channel PIEZO2. *Proc. Natl. Acad. Sci. U.S.A.* **119**, e2115821119 (2022).
12. B. Sorum, R. A. Rietmeijer, K. Gopakumar, H. Adesnik, S. G. Brohawn, Ultrasound activates mechanosensitive TRAAK K^+ channels through the lipid membrane. *Proc. Natl. Acad. Sci. U.S.A.* **118**, e2006980118 (2021).
13. Z. Qiu, J. Guo, S. Kala, J. Zhu, Q. Xian, W. Qiu, G. Li, T. Zhu, L. Meng, R. Zhang, H. C. Chan, H. Zheng, L. Sun, The mechanosensitive ion channel Piezo1 significantly mediates in vitro ultrasonic stimulation of neurons. *iScience* **21**, 448–457 (2019).
14. S.-J. Oh, J. M. Lee, H.-B. Kim, J. Lee, S. Han, J. Y. Bae, G.-S. Hong, W. Koh, J. Kwon, E.-S. Hwang, D. H. Woo, I. Youn, I.-J. Cho, Y. C. Bae, S. Lee, J. W. Shim, J.-H. Park, C. J. Lee, Ultrasonic neuromodulation via astrocytic TRPA1. *Curr. Biol.* **29**, 3386–3401.e8 (2019).
15. C. Constans, P. Mateo, M. Tanter, J.-F. Aubry, Potential impact of thermal effects during ultrasonic neurostimulation: Retrospective numerical estimation of temperature elevation in seven rodent setups. *Phys. Med. Biol.* **63**, 025003 (2018).
16. D. P. Darrow, P. O'Brien, T. J. Richner, T. I. Netoff, E. S. Ebbini, Reversible neuroinhibition by focused ultrasound is mediated by a thermal mechanism. *Brain Stimul.* **12**, 1439–1447 (2019).
17. R. L. King, J. R. Brown, W. T. Newsome, K. B. Pauly, Effective parameters for ultrasound-induced in vivo neurostimulation. *Ultrasound Med. Biol.* **39**, 312–331 (2013).
18. H. Kim, A. Chiu, S. D. Lee, K. Fischer, S.-S. Yoo, Focused ultrasound-mediated non-invasive brain stimulation: Examination of sonication parameters. *Brain Stimul.* **7**, 748–756 (2014).
19. B. Clennell, T. G. J. Steward, M. Elley, E. Shin, M. Weston, B. W. Drinkwater, D. J. Whitcomb, Transient ultrasound stimulation has lasting effects on neuronal excitability. *Brain Stimul.* **14**, 217–225 (2021).
20. K. Yoon, W. Lee, J. E. Lee, L. Xu, P. Croce, L. Foley, S.-S. Yoo, Effects of sonication parameters on transcranial focused ultrasound brain stimulation in an ovine model. *PLOS ONE* **14**, e0224311 (2019).
21. K. Yu, X. Niu, E. Krook-Magnuson, B. He, Intrinsic functional neuron-type selectivity of transcranial focused ultrasound neuromodulation. *Nat. Commun.* **12**, 2519 (2021).
22. T. Nandi, B. R. Kop, K. Butts Pauly, C. J. Stagg, L. Verhagen, The relationship between parameters and effects in transcranial ultrasonic stimulation. *Brain Stimul.* **17**, 1216–1228 (2024).
23. K. R. Murphy, J. S. Farrell, J. Bendig, A. Mitra, C. Luff, I. A. Stelzer, H. Yamaguchi, C. C. Angelakos, M. Choi, W. Bian, T. Dilanni, E. M. Pujol, N. Matosevich, R. Airan, B. Gaudillière, E. E. Konofagou, K. Butts-Pauly, I. Soltesz, L. De Lecea, Optimized ultrasound neuromodulation for non-invasive control of behavior and physiology. *Neuron* **112**, 3252–3266.e5 (2024).
24. K. Zeng, Z. Li, X. Xia, Z. Wang, G. Darmani, X. Li, R. Chen, Effects of different sonication parameters of theta burst transcranial ultrasound stimulation on human motor cortex. *Brain Stimul.* **17**, 258–268 (2024).
25. A. K. Zadeh, H. Raghuram, S. Shrestha, M. Kibreab, I. Kathol, D. Martino, G. B. Pike, S. Pichardo, O. Monchi, The effect of transcranial ultrasound pulse repetition frequency on sustained inhibition in the human primary motor cortex: A double-blind, sham-controlled study. *Brain Stimul.* **17**, 476–484 (2024).
26. B. R. Kop, Y. S. Oghli, T. C. Grippe, T. Nandi, J. Lefkes, S. W. Meijer, S. Farboud, M. Engels, M. Hamani, M. Null, A. Radetz, U. Hassan, G. Darmani, A. Chetverikov, H. E. M. Den Ouden, T. O. Bergmann, R. Chen, L. Verhagen, Auditory confounds can drive online effects of transcranial ultrasonic stimulation in humans. *Elife* **12**, RP88762 (2024).
27. H. Caffaratti, B. Slater, N. Shaheen, A. Rhone, R. Calmus, M. Kritikos, S. Kumar, B. Dlouhy, H. Oya, T. Griffiths, A. D. Boes, N. Trapp, M. Kaiser, J. Sallet, M. I. Banks, M. A. Howard, M. Zanaty, C. I. Petkov, Neuromodulation with ultrasound: Hypotheses on the directionality of effects and a community resource. *Elife* **13**, RP100827 (2024).
28. Y. Tufail, A. Matyushov, N. Baldwin, M. L. Tauchmann, J. Georges, A. Yoshihiro, S. I. H. Tillery, W. J. Tyler, Transcranial pulsed ultrasound stimulates intact brain circuits. *Neuron* **66**, 681–694 (2010).
29. Z. Wang, J. Yan, X. Wang, Y. Yuan, X. Li, Transcranial ultrasound stimulation directly influences the cortical excitability of the motor cortex in parkinsonian mice. *Mov. Disord.* **35**, 693–698 (2020).
30. Z. Li, R. Chen, D. Liu, X. Wang, W. Yuan, Effect of low-intensity transcranial ultrasound stimulation on theta and gamma oscillations in the mouse hippocampal CA1. *Front. Psychiatry* **14**, 1151351 (2023).
31. Y. Liu, G. Wang, C. Cao, G. Zhang, E. B. Tanzi, Y. Zhang, W. Zhou, Y. Li, Neuromodulation effect of very low intensity transcranial ultrasound stimulation on multiple nuclei in rat brain. *Front. Aging Neurosci.* **13**, 656430 (2021).
32. D. T. Nguyen, D. E. Berisha, E. E. Konofagou, J. P. Dmochowski, Neuronal responses to focused ultrasound are gated by pre-stimulation brain rhythms. *Brain Stimul.* **15**, 233–243 (2022).
33. R. Chen, A. Berardelli, A. Bhattacharya, M. Bologna, K.-H. S. Chen, A. Fasano, R. C. Helmich, W. D. Hutchison, N. Kamble, A. A. Kühn, A. Macerollo, W.-J. Neumann, P. K. Pal, G. Paparella, A. Suppa, K. Udupa, Clinical neurophysiology of Parkinson's disease and parkinsonism. *Clin. Neurophysiol. Pract.* **7**, 201–227 (2022).
34. C. Sarica, C. Iorio-Morin, D. H. Aguirre-Padilla, A. Najjar, M. Paff, A. Fomenko, K. Yamamoto, A. Zemmar, N. Lipsman, G. M. Ibrahim, C. Hamani, M. Hodaie, A. M. Lozano, R. P. Munhoz, A. Fasano, S. K. Kalia, Implantable pulse generators for deep brain stimulation: Challenges, complications, and strategies for practicality and longevity. *Front. Hum. Neurosci.* **15**, 708481 (2021).
35. C. Sarica, A. Fomenko, J.-F. Nankoo, G. Darmani, A. Vetkas, K. Yamamoto, A. M. Lozano, R. Chen, Toward focused ultrasound neuromodulation in deep brain stimulator implanted patients: Ex-vivo thermal, kinetic and targeting feasibility assessment. *Brain Stimul.* **15**, 376–379 (2022).
36. G. Darmani, H. Ramezanpour, C. Sarica, R. Annirood, T. Grippe, J.-F. Nankoo, A. Fomenko, B. Santyr, K. Zeng, A. Vetkas, N. Samuel, B. Davidson, A. Fasano, M. Lankarany, S. K. Kalia, S. Pichardo, A. M. Lozano, R. Chen, Individualized non-invasive deep brain stimulation of the basal ganglia using transcranial ultrasound stimulation. *Nat. Commun.* **16**, 2693 (2025).
37. N. Samuel, M. Y. R. Ding, C. Sarica, G. Darmani, I. E. Harmsen, T. Grippe, X. Chen, A. Yang, N. Nasrkhani, K. Zeng, R. Chen, A. M. Lozano, Accelerated transcranial ultrasound neuromodulation in Parkinson's disease: A pilot study. *Mov. Disord.* **38**, 2209–2216 (2023).
38. J.-F. Aubry, D. Attali, M. Schafer, E. Fouragnan, C. F. Caskey, R. Chen, G. Darmani, E. J. Bubrick, J. Sallet, C. R. Butler, C. J. Stagg, M. C. Klein-Flügge, S.-S. Yoo, C. Holland, B. Treeby, E. Martin, L. Verhagen, K. B. Pauly, ITRUSST consensus on biophysical safety for transcranial ultrasound stimulation. arXiv:2311.05359 [physics.bio-ph] (2023).
39. Z. Yin, G. Zhu, B. Zhao, Y. Bai, Y. Jiang, W.-J. Neumann, A. A. Kühn, J. Zhang, Local field potentials in Parkinson's disease: A frequency-based review. *Neurobiol. Dis.* **155**, 105372 (2021).
40. W. Neumann, A. A. Kühn, Subthalamic beta power—Unified Parkinson's disease rating scale III correlations require akinetic symptoms. *Mov. Disord.* **32**, 175–176 (2017).
41. Y. Chen, C. Gong, Y. Tian, N. Orlov, J. Zhang, Y. Guo, S. Xu, C. Jiang, H. Hao, W.-J. Neumann, A. A. Kühn, H. Liu, L. Li, Neuromodulation effects of deep brain stimulation on beta rhythm: A longitudinal local field potential study. *Brain Stimul.* **13**, 1784–1792 (2020).
42. N. Darcy, R. Lofredi, B. Al-Fatly, W.-J. Neumann, J. Hübl, C. Brücke, P. Krause, G.-H. Schneider, A. Kühn, Spectral and spatial distribution of subthalamic beta peak activity in Parkinson's disease patients. *Exp. Neurol.* **356**, 114150 (2022).
43. H. Iwaki, N. Nishikawa, M. Nagai, T. Tsujii, H. Yabe, M. Kubo, I. Ieiri, M. Nomoto, Pharmacokinetics of levodopa/benserazide versus levodopa/carbidopa in healthy subjects and patients with Parkinson's disease. *Neurol. Clin. Neurosci.* **3**, 68–73 (2015).
44. W. Legon, T. F. Sato, A. Opitz, J. Mueller, A. Barbour, A. Williams, W. J. Tyler, Transcranial focused ultrasound modulates the activity of primary somatosensory cortex in humans. *Nat. Neurosci.* **17**, 322–329 (2014).
45. A. Güngör, Ş. S. Baydın, V. M. Holanda, E. H. Middlebrooks, C. Isler, B. Tugcu, K. Foote, N. Tanriover, Microsurgical anatomy of the subthalamic nucleus: Correlating fiber dissection results with 3-T magnetic resonance imaging using neuronavigation. *J. Neurosurg.* **130**, 716–732 (2019).
46. M. Chikermane, L. Weerdmeester, N. Rajamani, R. M. Köhler, T. Merk, J. Vanhoecke, A. Horn, W. J. Neumann, Cortical beta oscillations map to shared brain networks modulated by dopamine. *Elife* **13**, RP97184 (2024).
47. A. A. Kuhn, F. Kempf, C. Brucke, L. Gaynor Doyle, I. Martinez-Torres, A. Pogosyan, T. Trottenberg, A. Kupsch, G.-H. Schneider, M. I. Hariz, W. Vandenberghe, B. Nuttin, P. Brown, High-frequency stimulation of the subthalamic nucleus suppresses oscillatory activity in patients with Parkinson's disease in parallel with improvement in motor performance. *J. Neurosci.* **28**, 6165–6173 (2008).
48. A. W. Shukla, J. J. Shuster, J. W. Chung, D. E. Vaillancourt, C. Patten, J. Ostrem, M. S. Okun, Repetitive transcranial magnetic stimulation (rTMS) therapy in Parkinson disease: A meta-analysis. *PM R* **8**, 356–366 (2016).
49. A. Zanjani, K. K. Zakzanis, Z. J. Daskalakis, R. Chen, Repetitive transcranial magnetic stimulation of the primary motor cortex in the treatment of motor signs in Parkinson's disease: A quantitative review of the literature. *Mov. Disord.* **30**, 750–758 (2015).
50. M. Y. R. Ding, T. Arora, C. Sarica, A. Z. Yang, N. Nasrkhani, T. Grippe, J.-F. Nankoo, S. Tran, N. Samuel, X. Xia, A. M. Lozano, R. Chen, Investigation of metaplasticity associated with transcranial focused ultrasound neuromodulation in humans. *J. Neurosci.* **44**, e2438232024 (2024).
51. N. Samuel, K. Zeng, I. E. Harmsen, M. Y. R. Ding, G. Darmani, C. Sarica, B. Santyr, A. Vetkas, A. Pancholi, A. Fomenko, V. Milano, K. Yamamoto, U. Saha, R. Wennberg, N. C. Rowland,

R. Chen, A. M. Lozano, Multi-modal investigation of transcranial ultrasound-induced neuroplasticity of the human motor cortex. *Brain Stimul.* **15**, 1337–1347 (2022).
52. T. Grippe, Y. Shamli-Oghli, G. Darmani, J. Nankoo, N. Raies, C. Sarica, T. Arora, C. Gunraj, M. Y. R. Ding, C. Rinchon, D. G. DiLuca, S. Pichardo, F. Cardoso, A. M. Lozano, R. Chen, Plasticity-induced effects of theta burst transcranial ultrasound stimulation in Parkinson's disease. *Mov. Disord.* **39**, 1364–1374 (2024).
53. H.-J. Kim, T. T. Phan, K. Lee, J. S. Kim, S.-Y. Lee, J. M. Lee, J. Do, D. Lee, S.-P. Kim, K. P. Lee, J. Park, C. J. Lee, J. M. Park, Long-lasting forms of plasticity through patterned ultrasound-induced brainwave entrainment. *Sci. Adv.* **10**, eadk3198 (2024).
54. P.-Y. Fong, B. R. Kop, C. Evans, V. G. Wijaya, Y. Lin, D. Cappotto, J. S. A. Lee, A. Latorre, J. Song, B. Treeby, E. Martin, J. Rothwell, L. Verhagen, S. Bestmann, Failed double-blind replication of offline 5Hz-rTUS-induced corticospinal excitability. bioRxiv 2024.11.25.625187 [Preprint] (2024). https://doi.org/10.1101/2024.11.25.625187.
55. C. Atkinson-Clement, M. Alkhawashki, M. Gatica, S. A. Kontogouris, M. Kaiser, Delay- and pressure-dependent neuromodulatory effects of transcranial ultrasound stimulation. *Neuromodulation* **28**, 444–454 (2025).
56. C. Atkinson-Clement, M. Alkhawashki, M. Gatica, J. Ross, M. Kaiser, Dynamic changes in human brain connectivity following ultrasound neuromodulation. *Sci. Rep.* **14**, 30025 (2024).
57. S. N. Yaakub, T. A. White, J. Roberts, E. Martin, L. Verhagen, C. J. Stagg, S. Hall, E. F. Fouragnan, Transcranial focused ultrasound-mediated neurochemical and functional connectivity changes in deep cortical regions in humans. *Nat. Commun.* **14**, 5318 (2023).
58. D. Keeser, L. Roell, V. Meedt, M. Haßlberger, M. Korman, E. Schulz, M. Lueckel, B. Karsli, G. Hasanaj, T. Faeßler, G. Vural, K.-Y. Chang, L. Bulubas, F. Padberg, F. Raabe, P. Falkai, T. O. Bergmann, B.-S. Rauchmann, Modulating brain perfusion, functional connectivity, and metabolite patterns through theta burst transcranial ultrasonic stimulation. bioRxiv 2025.06.25.661571 [Preprint] (2025). https://doi.org/10.1101/2025.06.25.661571.
59. K. Nakajima, T. Osada, A. Ogawa, M. Tanaka, S. Oka, K. Kamagata, S. Aoki, Y. Oshima, S. Tanaka, S. Konishi, A causal role of anterior prefrontal-putamen circuit for response inhibition revealed by transcranial ultrasound stimulation in humans. *Cell Rep.* **40**, 111197 (2022).
60. A. In, A. Strohman, B. Payne, W. Legon, Low-intensity focused ultrasound to the posterior insula reduces temporal summation of pain. *Brain Stimul.* **17**, 911–924 (2024).
61. Y. Shamli Oghli, T. Grippe, T. Arora, T. Hoque, G. Darmani, R. Chen, Mechanisms of theta burst transcranial ultrasound induced plasticity in the human motor cortex. *Brain Stimul.* **16**, 1135–1143 (2023).
62. V. Mathiopoulou, R. Lofredi, L. K. Feldmann, J. Habets, N. Darcy, W.-J. Neumann, K. Faust, G.-H. Schneider, A. A. Kühn, Modulation of subthalamic beta oscillations by movement, dopamine, and deep brain stimulation in Parkinson's disease. *NPJ Parkinsons Dis.* **10**, 77 (2024).
63. G. Tinkhauser, A. Pogosyan, S. Little, M. Beudel, D. M. Herz, H. Tan, P. Brown, The modulatory effect of adaptive deep brain stimulation on beta bursts in Parkinson's disease. *Brain* **140**, 1053–1067 (2017).
64. K. Horváth, Z. Aschermann, P. Ács, G. Deli, J. Janszky, S. Komoly, É. Balázs, K. Takács, K. Karádi, N. Kovács, Minimal clinically important difference on the motor examination part of MDS-UPDRS. *Parkinsonism Relat. Disord.* **21**, 1421–1426 (2015).
65. Y.-Y. Lin, N. Raies, T. Grippe, C. A. Gunraj, C. Sarica, U. K. Saha, A. Bhattacharya, G. Darmani, R. Chen, Transcranial ultrasound stimulation of internal globus pallidus region and motor cortex in Parkinson's disease. *Mov. Disord.* **41**, 416–425 (2026).
66. M. Mohammadjavadi, R. T. Ash, G. H. Glover, K. B. Pauly, Optimization of MR-ARFI for human transcranial focused ultrasound. bioRxiv 2024.11.13.623314 [Preprint] (2024). https://doi.org/10.1101/2024.11.13.623314.
67. E. Martin, M. Roberts, I. F. Grigoras, O. Wright, T. Nandi, S. W. Rieger, J. Campbell, T. Den Boer, B. T. Cox, C. J. Stagg, B. E. Treeby, Ultrasound system for precise neuromodulation of human deep brain circuits. *Nat. Commun.* **16**, 8024 (2025).
68. K. Yu, B. He, Transcranial focused ultrasound modulates visual thalamus in a nonhuman primate model. *IEEE Trans. Biomed. Eng.* **72**, 2893–2901 (2025).
69. J. Kosnoff, K. Yu, C. Liu, B. He, Transcranial focused ultrasound to V5 enhances human visual motion brain-computer interface by modulating feature-based attention. *Nat. Commun.* **15**, 4382 (2024).
70. C. Atkinson-Clement, M. Kaiser, M. A. Lambon Ralph, J. Jung, Ventricle stimulation as a potential gold-standard control stimulation site for transcranial focused ultrasound stimulation. *Brain Stimul.* **17**, 1328–1330 (2024).
71. V. Mathiopoulou, J. Habets, L. K. Feldmann, J. L. Busch, J. Roediger, J. K. Behnke, G.-H. Schneider, K. Faust, A. A. Kühn, Gamma entrainment induced by deep brain stimulation as a biomarker for motor improvement with neuromodulation. *Nat. Commun.* **16**, 2956 (2025).
72. A. Rezai, M. Ranjan, A. Bhagwat, T. Arsiwala, J. Carpenter, M. Schafer, G. Adams, J. Marton, P. Tirumalai, D. Farmer, J. Mahoney, V. Finomore, Brain injury during focused ultrasound neuromodulation for substance use disorder. *Brain Stimul.* **18**, 2050–2053 (2025).
73. A. Rezai, M. Ranjan, A. Bhagwat, T. Arsiwala, J. Carpenter, M. Schafer, G. Adams, J. Marton, P. Tirumalai, D. Farmer, J. Mahoney, V. Finomore, Further clarification regarding brain injury during focused ultrasound neuromodulation for substance use disorder. *Brain Stimul.* **19**, 103014 (2026).
74. J. Herron, A. Kullmann, T. Denison, W. K. Goodman, A. Gunduz, W.-J. Neumann, N. R. Provenza, M. M. Shanechi, S. A. Sheth, P. A. Starr, A. S. Widge, Challenges and opportunities of acquiring cortical recordings for chronic adaptive deep brain stimulation. *Nat. Biomed. Eng* **9**, 606–617 (2025).
75. N. M. Rotstein, Z. D. Cohen, A. Welborn, T. D. Zbozinek, S. Akre, K. G. Jones, K. E. Null, J. Pontanares, K. L. Sanchez, D. C. Flanagan, S. E. Halavi, E. Kittle, M. G. McClay, A. A. T. Bui, K. L. Narr, R. C. Welsh, M. G. Craske, T. P. Kuhn, Investigating low intensity focused ultrasound pulsation in anhedonic depression—A randomized controlled trial. *Front. Hum. Neurosci.* **19**, 1478534 (2025).
76. J. Jung, C. Atkinson-Clement, M. Kaiser, M. A. Lambon Ralph, Transcranial focused ultrasound stimulation of the anterior temporal lobe enhances semantic memory by modulating brain morphology, neurochemistry and neural dynamics. bioRxiv 2025.03.10.642483 [Preprint] (2025). https://doi.org/10.1101/2025.03.10.642483.
77. S. Clarke, S. Mugglestone, M. Lojkiewiez, J. Marquez, N. Bault, E. Fouragnan, S. Hughes, Multi-focal ultrasound neuromodulation to the dorsal anterior cingulate cortex disrupts behavioural and neural pain processing. bioRxiv 2025.09.04.674195 [Preprint] (2025). https://doi.org/10.1101/2025.09.04.674195.
78. A. I. Sonmez, D. D. Camsari, A. L. Nandakumar, J. L. V. Voort, S. Kung, C. P. Lewis, P. E. Croarkin, Accelerated TMS for depression: A systematic review and meta-analysis. *Psychiatry Res.* **273**, 770–781 (2019).
79. U. Ozer, B. Yucens, S. Tumkaya, Efficacy of accelerated deep transcranial magnetic stimulation with double cone coil in obsessive-compulsive disorder: A double-blind, placebo-controlled study. *J. Psychiatr. Res.* **171**, 325–331 (2024).
80. A. Strohman, B. Payne, A. In, K. Stebbins, W. Legon, Low-intensity focused ultrasound to the human dorsal anterior cingulate attenuates acute pain perception and autonomic responses. *J. Neurosci.* **44**, e1011232023 (2024).
81. S. G. J. Boccard, E. A. C. Pereira, L. Moir, T. Z. Aziz, A. L. Green, Long-term outcomes of deep brain stimulation for neuropathic pain. *Neurosurgery* **72**, 221–231 (2013).
82. A. A. Bari, A. Fasano, R. P. Munhoz, A. M. Lozano, Improving outcomes of subthalamic nucleus deep brain stimulation in Parkinson's disease. *Expert Rev. Neurother.* **15**, 1151–1160 (2015).
83. P. Temperli, J. Ghika, J.-G. Villemure, P. R. Burkhard, J. Bogousslavsky, F. J. G. Vingerhoets, How do parkinsonian signs return after discontinuation of subthalamic DBS? *Neurology* **60**, 78–81 (2003).
84. M. H. Trager, M. M. Koop, A. Velisar, Z. Blumenfeld, J. S. Nikolau, E. J. Quinn, T. Martin, H. Bronte-Stewart, Subthalamic beta oscillations are attenuated after withdrawal of chronic high frequency neurostimulation in Parkinson's disease. *Neurobiol. Dis.* **96**, 22–30 (2016).
85. L. K. Feldmann, R. Lofredi, W.-J. Neumann, B. Al-Fatly, J. Roediger, B. H. Bahners, P. Nikolov, T. Denison, A. Saryyeva, J. K. Krauss, K. Faust, E. Florin, A. Schnitzler, G.-H. Schneider, A. A. Kühn, Toward therapeutic electrophysiology: Beta-band suppression as a biomarker in chronic local field potential recordings. *NPJ Parkinsons Dis.* **8**, 44 (2022).
86. B. B. Avants, N. J. Tustison, G. Song, P. A. Cook, A. Klein, J. C. Gee, A reproducible evaluation of ANTs similarity metric performance in brain image registration. *Neuroimage* **54**, 2033–2044 (2011).
87. E. T. Rolls, C.-C. Huang, C.-P. Lin, J. Feng, M. Joliot, Automated anatomical labelling atlas 3. *Neuroimage* **206**, 116189 (2020).
88. E. Martin, J.-F. Aubry, M. Schafer, L. Verhagen, B. Treeby, K. B. Pauly, ITRUSST consensus on standardised reporting for transcranial ultrasound stimulation. *Brain Stimul.* **17**, 607–615 (2024).
89. S. Pichardo, BabelBrain: An open-source application for prospective modeling of transcranial focused ultrasound for neuromodulation applications. *IEEE Trans. Ultrason. Ferroelectr. Freq. Control* **70**, 587–599 (2023).
90. Y. Thenaisie, K. Lee, C. Moerman, S. Scafa, A. Gálvez, E. Pirondini, M. Burri, J. Ravier, A. Puiatti, E. Accolla, B. Wicki, A. Zacharia, M. Castro Jiménez, J. F. Bally, G. Courtine, J. Bloch, E. M. Moraud, Principles of gait encoding in the subthalamic nucleus of people with Parkinson's disease. *Sci. Transl. Med.* **14**, eabo1800 (2022).
91. R. Oostenveld, P. Fries, E. Maris, J.-M. Schoffelen, FieldTrip: Open source software for advanced analysis of MEG, EEG, and invasive electrophysiological data. *Comput. Intell. Neurosci.* **2011**, 1–9 (2011).
92. G. Tinkhauser, A. Pogosyan, H. Tan, D. M. Herz, A. A. Kühn, P. Brown, Beta burst dynamics in Parkinson's disease OFF and ON dopaminergic medication. *Brain* **140**, 2968–2981 (2017).
93. C. Neudorfer, K. Butenko, S. Oxenford, N. Rajamani, J. Achtzehn, L. Goede, B. Hollunder, A. S. Ríos, L. Hart, J. Tasserie, K. B. Fernando, T. A. K. Nguyen, B. Al-Fatly, M. Vissani, M. Fox, R. M. Richardson, U. Van Rienen, A. A. Kühn, A. D. Husch, E. Opri, T. Dembek, N. Li, A. Horn, Lead-DBS v3.0: Mapping deep brain stimulation effects to local anatomy and global networks. *Neuroimage* **268**, 119862 (2023).
94. C. Sarica, K. Yamamoto, A. Loh, G. J. B. Elias, A. Boutet, R. Madhavan, J. Germann, A. Zemmar, D. Gwun, J. Tasserie, D. M. Andrade, M. Hodaie, S. K. Kalia, R. A. Wennberg,

A. M. Lozano, Blood oxygen level-dependent (BOLD) response patterns with thalamic deep brain stimulation in patients with medically refractory epilepsy. *Epilepsy Behav.* **122**, 108153 (2021).
95. R. N. Henson, H. Abdulrahman, G. Flandin, V. Litvak, Multimodal integration of M/EEG and f/MRI data in SPM12. *Front. Neurosci.* **13**, 300 (2019).
96. B. L. Edlow, A. Mareyam, A. Horn, J. R. Polimeni, T. Witzel, M. D. Tisdall, J. C. Augustinack, J. P. Stockmann, B. R. Diamond, A. Stevens, L. S. Tirrell, R. D. Folkerth, L. L. Wald, B. Fischl, A. Van Der Kouwe, 7 Tesla MRI of the ex vivo human brain at 100 micron resolution. *Sci. Data* **6**, 244 (2019).

Acknowledgments: We sincerely thank C. Gunraj, U. Saha, and J. Kwok for technical support and assistance with regulatory matters and A. Naheed for conducting the MRI scans of the patients. **Funding:** This work was funded by the Alan & Susan Hudson Cornerstone Chair in Neurosurgery at University Health Network to A.M.L., Canadian Institutes of Health Research (FDN 154292, ENG 173742, and PJT 198046 to R.C.), and Weston Brain Institute (TR201348 to A.M.L.). **Author contributions:** C.S., G.D., H.R., S.K.K., A.A., A.M.L., and R.C. conceptualized and designed the project. C.S., G.D., T.C., R.A., N.R., J.-F.N., N.S., M.Y.R.D., A.V., A. Fomenko, M.H., R.P.M., and A. Fasano contributed to patient recruitment, data acquisition during study visits, and institutional ethics board approvals. C.S., G.D., and H.R. performed all data analyses and generated all figures. M.C. performed blinded video evaluations. B.S. performed electrode modeling. S.P. designed the ultrasound modeling software and assisted with ultrasound simulations. J.D.S. critically revised the manuscript. A.M.L. and R.C. acquired funding, administered the project, and supervised the study. C.S., G.D., and H.R. wrote the manuscript with input from all authors. All coauthors approved the final manuscript. **Competing interests:** C.S. has been receiving fellowship grants from the Michael and Amira Dan Foundation and Turkish Neurosurgical Society. A.M.L. is scientific director for the Functional Neuromodulation and a consultant to Medtronic, Abbott, Boston Scientific, Insightec, and Focused Ultrasound Foundation. A.F. reports the following: consultancies from Abbvie, Medtronic, Boston Scientific, Sunovion, Merz, UCB, and Ipsen; membership in advisory boards of Abbvie, Boston Scientific, Ceregate, Inbrain, and Inbrain Pharma; receiving honoraria from Abbvie, Medtronic, Boston Scientific, Sunovion, Merz, UCB, and Ipsen; and receiving grants from Dystonia Medical Research Foundation, MSA Coalition, University of Toronto, Weston Foundation, Abbvie, Medtronic, and Boston Scientific. S.K.K. receives honoraria, consulting, and speaker fees from Abbott, Boston Scientific, inBrain, Medtronic, Novo Nordisk, Parkinson Canada, and Movement Disorders Society and research support from Parkinson Canada, CIHR, MJFF, FUS Foundation, MitoO2, Toronto Western Hospital Foundation, Weston Foundation, and RR Tasker Chair in Stereotactic and Functional Neurosurgery. R.C. was a consultant for Attune Neuroscience. The other authors declare that they have no competing interests. **Data, code, and materials availability:** All data associated with this study are present in the paper or the Supplementary Materials. Raw data can be made available upon reasonable request under a data transfer agreement with G.D. (ghazaleh.darmani@uhn.ca) to ensure compliance with participant consent and data protection regulations. All materials newly generated in this study are commercially available or will be available upon reasonable request.

Submitted 6 July 2025
Resubmitted 7 December 2025
Accepted 30 March 2026
Published 20 May 2026
10.1126/scitranslmed.ady1883

Science Translational Medicine

Transcranial ultrasound stimulation of motor networks in Parkinson's disease informed by local field potential dynamics

Can Sarica, Ghazaleh Darmani, Hamidreza Ramezanpour, Marcus Callister, Brendan Santyr, Talyta Grippe, Regina Annirood, Nasem Raies, Jean-Francois Nankoo, Nardin Samuel, Mandy Yi Rong Ding, Artur Vetkas, Anton Fomenko, Jeffrey D. Schall, Mojgan Hodaie, Suneil K. Kalia, Agessandro Abrahao, Renato P. Munhoz, Alfonso Fasano, Samuel Pichardo, Robert Chen, and Andres M. Lozano

Sci. Transl. Med. **18** (850), eady1883. DOI: 10.1126/scitranslmed.ady1883

Editor's summary

Transcranial ultrasound stimulation (TUS) is a noninvasive neuromodulation technique that allows targeting of superficial as well as deep brain regions and is therefore a potential treatment avenue for Parkinson's disease (PD). Successful clinical application of TUS requires a better understanding of target-specific network effects in the context of disease. In an exploratory clinical study, Sarica *et al.* examined the effects of TUS on subthalamic nucleus (STN) local field potentials in 17 patients with Parkinson's disease. TUS of the motor cortex suppressed beta activity in the STN and resulted in a modest but significant improvement of MDS-UPDRS-III scores 50 minutes after TUS, whereas TUS of the globus pallidus internus enhanced beta power without clinical benefit. These findings highlight the motor cortex as a potential TUS brain target for PD. —Daniela Neuhofer